Chapter 7

Upper Atmospheric Wind and Temperature Measurements using Imaging Fabry-Perot Interferometers

David Rees, Ian McWhirter, Anasuya Aruliah and Simon Batten,

Atmospheric Physics Laboratory,
Department of Physics and Astronomy,
University College London,
Gower Street, London WC1E 6BT, UK

Abstract.

The Fabry-Perot interferometer is a high resolution spectrometer which has a relatively large etendue for a given instrument size and cost, and has thus been very widely used for aeronomic studies, particularly those involving visible and near-IR airglow and auroral emissions. The performance of the classical FPI, however, has been quite critically limited by the normal use of a 'pinhole' detector, namely the photomultiplier. The development of two-dimensional Imaging Photon Detectors provided a very effective means of considerably increasing the sensitivity, thus improving the performance, and of simultaneously reducing the complexity of a Fabry-Perot Interferometer (FPI). These gains have been particularly important for instruments located at remote stations, making upper atmospheric wind and related measurements. Two forms of this Imaging FPI have been developed and deployed by the Atmospheric Physics Laboratory at University College London. The standard Imaging FPI, of which some 10 instruments are now in routine operation at 7 (mainly high-latitude) stations, has a 15 cm clear aperture etalon. One complete Fabry-Perot fringe is continuously imaged and recorded, and the viewing direction is scanned around the sky, through 8 discrete directions, including zenith. The Imaging FPI system has a significant multiplex advantage over non-imaging FPIs (where the optical path difference is scanned, and a pinhole sampler is used), since the entire available signal is recorded all the time. In the Doppler Imaging System (DIS), an all-sky optical imaging system is used ahead of the FPI, to avoid entirely the requirement of a physical scanning system. In the DIS, typically 5 fringes are imaged onto the 2-dimensional detector, further increasing the multiplex gain, while providing a full and continuous 2-dimensional representation of a large upper atmospheric region (400 km radius for the thermospheric OI red line) centred on the observing station. In excess of 2000 nights of useful thermospheric data have been obtained with this class of ground-based instrument since late 1980. The latest improvement with the systems involves the deployment of Imaging Photon Detectors with Gallium Arsenide photocathodes. A recently-deployed system with such a detector has opened up the near-I.R. to FPI observations, initially using the OH Mienel emissions near 840 nm for mesospheric wind and temperature measurements. Some exciting possibilities of imaging two-dimensional wind and temperature fields in the mesosphere, and in the lower and upper thermosphere, will be realised as these GaAs IPDs become more widely available. Some of the highlights of the observations from the Imaging FPIs and DIS will be used to illustrate the capabilities of the instruments.

1. Introduction

The conventional Fabry-Perot interferometer, as used for ground-based studies of upper atmospheric winds and temperature, has used a pinhole detector to detect the optical signal, while the Optical Path Difference (OPD) of the etalon is changed by pressure-scanning (change of refractive index) the etalon cavity, or by mechanical scanning of the etalon plate separation. These instruments have been widely used since the 1960's (Armstrong 1968), and the methodology is widely reported in the literature, and reviewed by Hernandez (1986), Meriwether (1984, 1989) and Meriwether et al., (1986).

A fundamental limitation of the conventional FPI is the severe restriction on the acceptable solid angle, i.e. that which can be transmitted to a detector without degrading the spectral transmission of the instrument (the Jacquinot criterion). A number of attempts have been made, using photographic methods, image intensifiers, multiple element masks etc, to 'field-widen' the FPI, thus increasing the entendue and thus throughput. However, these were never entirely successful in the context of an 'observatory class instrument', since they usually demanded a considerable effort to build and align the instrument, and a great deal of effort to calibrate, maintain stability, and then analyse the data. Several of the methods which reached the stage of being initially deployed in the field, but not of becoming widely and reliably used, were reviewed by Hernandez (1986).

Two fundamental requirements had to be defined and then solved experimentally in the development of a truly successful instrument capable of overcoming these limitations to the FPI.

Firstly, it required the development of a relatively cheap, compact, simple and reliable two-dimensional Imaging Photon Detector (IPD) of high optical performance and excellent medium and long-term image and photometric stability. A 5-year development programme at UCL, started in 1975, produced the first IPDs which met these requirements in 1979, although very considerable technical and performance improvements have been made since then (McWhirter et al., 1982; Rees et al., 1985, 1986, 1989). One of the major, unsung, advantages of the IPD over other available imaging detectors is the extremely low noise associated with the devices. At the very low detectable signal levels which characterise all aeronomic interferometric measurements, it is not so much the detective quantum efficiency itself which limits performance, but a complex ratio of DQE to read-out and thermal electron noise. This factor will not be discussed in detail here, however, the absence of any read-out noise for the IPD, coupled with a thermal electron noise of 0.01 photon-equivalent event per 60 sec per pixel, and no susceptibility to cosmic ray events ensures that it is only the 'square root "n"' of the detected signal itself which contributes to limiting the instrument performance under given very low signal level conditions. This factor is of extreme importance for determining limiting performance / signal levels for airglow studies, in particular.

Secondly, it required the development of a very stable and rugged Fabry-Perot etalon, including the necessary mounting and other structures, so that a non-scanned imaging instrument could be built. The key factor here, which otherwise may not be obvious, is that the regular scanning of the OPD does provide a regular auto-calibration of the FPI. In a non-scanning, imaging system, other methods of calibration of the OPD and other parameters have to be developed and utilised. The Fabry-Perot etalon technology was developed in conjunction with I.C. Optical Systems of London, in a programme starting in 1970 / 71. This programme was aimed at the development of rocket and satellite-borne FPIs, and was exploited with several successful rocket flights of UCL FPIs in the mid 1970s and early 1980s; in a collaboration with the University of Michigan in which UCL developed and provided the flight etalons of the DE-2 Fabry-Perot interferometer; in two high altitude balloon flights of the UCL triple-etalon FPI (1980 and 1983) which demonstrated the technique of stratospheric wind measurements from interferometric observations of molecular absorption-lines; and in the development of prototypes of etalons for the High Resolution Doppler Interferometer of the NASA Upper Atmosphere Research Satellite (Rees 1979; Kaskiewicz 1978; Rees et al., 1982; Killeen et al., 1982; Rees et al., 1983, 1984).

There was also a third, implicit, limitation before the mid 1970s, associated with on-line data handling. The two-dimensional detectors provide a challenge for a non computer-based signal processing system,

in terms of electronic complexity, development time and cost. The advent of machines based on the 8080 / 8085, and comparable microprocessor chips revolutionised the design of the signal processing system required for the Imaging Fabry-Perot interferometers. By 1980/81, software to run these machines had been implemented on 8085 and 6502-based personal computers, and on DEC 11-23 machines. These machines, for the first time, allowed the software and straightforward serial / parallel interfaces to carry out all the functions of instrument control, timing, data input, processing, display and storage.

The rapid advent of personal computers, during 1981/2/3, provided another major boost to the cost-effectiveness of these instruments. PCs provide an immediate solution encompassing a convenient programming environment, very cost-effective computational power and data storage, flexible interfacing, the capability of auto-start and re-boot using back-up internal clocks and inbuilt reliable hard disk facilities for the operating system and software and for data storage. The global availability of systems, servicing and spares also completely changed the nature of the limitations to the sophistication of the overall instrument and its operating system: since the computer replaced a very complex and by its nature relatively unreliable and difficult to repair controller system, it rapidly became possible to build a very simple and reliable controller and power supply unit, set through its many functions by a very cheap and reliable personal computer. With regular data back-up, even a complete disk crash, nearly the worst scenario, can be solved for all but one of our instruments by a visit to the local and friendly personal computer supermarket. For the outstanding instrument, at Halley Bay, Antarctica, the only solution to problems is still an abundant supply of spare parts and instruction manuals. The very considerable simplification of the electronics, and the easy general availability of the PC made the 'cloning' of such instruments an attractive possibility, when coupled with the demonstrated high performance and combination of reliability and ruggedness in operation.

The Imaging Fabry-Perot interferometers (FPI) have been widely used to study the motion of the middle and upper thermosphere by measuring Doppler shifts of the OI 630.0 nm emission (Rees et al., 1984, 1985, 1987; Smith et al., 1985; Meriwether et al., 1986; Stewart et al., 1988). Similarly, neutral winds in the lower thermosphere may be derived, under the proper observing conditions (in particular, lack of auroral contamination), from Doppler shifts of the OI 557.7 nm emission. Such measurements, on a routine basis, have been extremely useful for describing the neutral dynamics within the thermosphere. Both middle / upper thermosphere and lower thermosphere observations provide a useful input for the thermospheric general circulation models (TGCM). They also supply an independent measurement of the winds in the lower thermosphere for comparison with the data from incoherent and partial reflection radars.

There have been previous attempts at interferometric Doppler wind studies of the OH Mienel emissions near 840 nm. The early versions of the IPD had photocathodes characterised by S-20 response, with the occasional device reaching the S-25 specification (extended red response). Due to the relatively high cost of the IPD (the 'cheap' being relative to similar detectors for Astronomy and Space Science applications), it was, until recently, necessary to run them in a conservative way, with a significant reduction in Detective Quantum efficiency. Lately, devices with a full S-25 photocathode specification have become available from ITT (USA). ITT have also started production (currently very limited numbers) of IPDs with Gallium Arsenide (GaAs) windows. These latter devices, in particular, have completely revolutionised interferometric studies of near IR airglow emissions such as OH. Some examples of recent very successful OH studies, and thus of winds near 85 km altitude, will be discussed later.

This first exploration of the region around 850 nm will be followed by further forays, using ground-based instruments, to study even weaker emissions, well below previously achievable thresholds. One of the limitations from the ground is, however, the relatively high near IR background night-glow continuum (or quasi-continuum), mainly of atmospheric origin. From space-borne instruments observing the atmosphere at the limb, the background intensity level is usually much lower. The intensity of specific emission features is considerably enhanced by the Van Rhijn effect. Thus there are considerable possibilities for future development and exploitation of these techniques and instruments. While space-borne instruments have the greatest potential, via their capability for global coverage, the number of future space-borne instruments will be quite limited due to the high cost and limited

number of suitable space platforms. Ground-based instruments will thus continue to have a significant role in the future investigation of upper atmospheric dynamics, in particular.

2: Instrument Description.

I: The Imaging Fabry-Perot Interferometer.

The group of Imaging Fabry-Perot Interferometers developed by the University College London Atmospheric Physics Laboratory is primarily intended to measure upper atmospheric winds via the Doppler shift of the same airglow and auroral emissions as those used by conventional Ground-based Fabry-Perot interferometer instruments (i.e. Meriwether, 1989). The major distinction has been the exploitation of a two-dimensional Imaging Photon Detector (McWhirter et al., 1982), to take advantage of a multiplex gain, reading the entire Fabry-Perot Fringe pattern continuously, rather than sequentially stepping through the spectrum by changing the Optical Path Difference (OPD), and thus being limited to deploying only a small, on-axis, sampling aperture.

The complete instrument is illustrated schematically in Figure 1. The FPI comprises a scanning mirror system, the F-P etalon, a focussing telescope, an interference filter, the detector and a spectral calibration source. These components are mounted from a rigid and rugged four-bar optical bench, to ensure that the alignment and focus of the entire system is maintained. The entire instrument, sealed by light-tight covers, is normally mounted within an enclosure which is dark and light-tight and thermally controlled to within about 3 - 5^{o} C. As for most of these FPI instruments, a plexiglass dome provides access to the night sky. The system is completed by an electronic controller unit (ECU), run from a fairly standard IBM PC (XT or upward in specification), the detector signal processing unit (SPU), and a thermal control system for the detector. The latter is normally a power supply for the Peltier cooler built into the detector, and a cooler / pump for removing heat from the hot junction of the Peltier elements via a liquid (water) system.

The etalons of the Imaging FPIs (for the OI 557 or 630 nm emission) have a nominal 14 mm gap and a 15 cm diameter clear, working, aperture. The three spacers of the etalon are made of zerodur, so that the thermal expansion coefficient of the etalon is of the order of 0.2 - 0.4 $10^{-6}K^{-1}$. The etalon itself, mounted within a sealed and evacuated container, is temperature-stablised to +/- O.1 K, so that the Optical Path Difference is not affected by changes of ambient air pressure and refractive index. Further details of the etalon design and other instrument details can be found in Rees et al. (1982) and Rees et al. (1984). The appropriate spectral region required for a specific investigation is normally selected with a 1 nm interference filter, to reduce unwanted contamination from night-sky continuum, or from other nearby airglow or auroral line or band emissions. Usually, about 1.0 to 1.5 fringes, corresponding to a field of view of about 1.0^{o}, are imaged by a telescope (lens or Cassegrain) of suitable focal length onto the photocathode of the Imaging Photon Detector. The IPD photocathode has a diameter of either 18 or 25 mm. The detector uses a resistive anode as the position-sensing technique, described elsewhere by Rees et al., (1980, 1981) and McWhirter et al, (1982). For each detected photon, the detector's output signals are converted by analogue computation into a 256 by 256 digital (x,y) image coordinate representation. These data are stored in computer memory, where the full 2-D image is normally built up, with a 16 bit counter allocation for each pixel in the image array. The nominal wavelength resolution of one image pixel is wavelength and instrument-dependent, but is of the order of 0.2 pm. This translates, typically, to an equivalent Doppler shift of around 100 ms^{-1}. To maintain instrument stability the temperature of the etalon container is actively controlled to better than 0.1 Celsius, at a temperature a few degrees above the highest anticipated observatory temperature.

In recently-built FPIs, detectors of high red-sensitivity using Gallium Arsenide (GaAs) photocathodes have been used to provide a greatly improved response to the OI 630 nm emission, and to those emissions such as OII 730 nm and OH 840 nm which are even further into the near IR. It is essential to cool the photocathodes of such detectors to -20C or -30C, to reduce the thermionic emission to a negligible level. A Peltier cooler is used, with the hot junction being cooled by a circulating water system. Depending on the requirements, this circulating water system is itself cooled or thermally

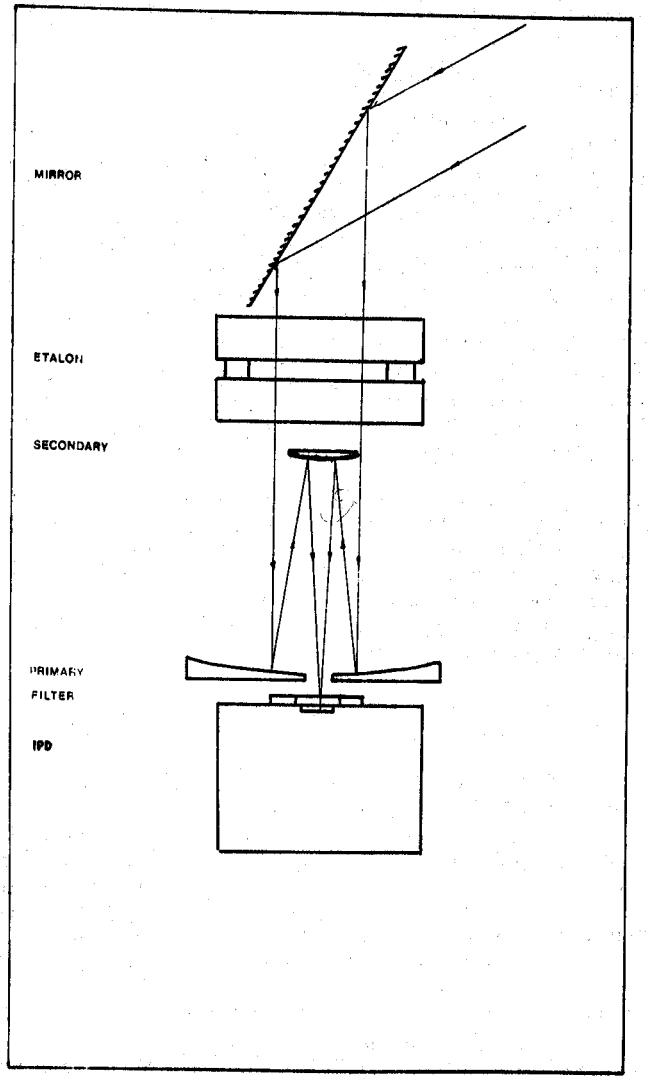

Figure 1: A schematic diagram of the Imaging Fabry-Perot Interferometer, showing how the component parts are arranged within the instrument, and the path of light rays through the instrument.

controlled, to maintain the stability of the detector photocathode temperature. This Peltier cooler is specially designed for the format of the particular IPD. In practice, the water-backed systems have proven rather more reliable than air-cooled versions. Ensuring the combination of a good air circulation and zero light leakage is a particular problem with air-cooled Peltier systems.

II: The Doppler Imaging System.

The UCL Doppler Imaging System is presently operating from the optical station at the Swedish Institute for Space Studies (IRF). It is a Fabry-Perot interferometer of high spectroscopic resolution with two major modifications. Firstly, a high resolution, two-dimensional, Imaging Photon Detector (IPD), (McWhirter et al., 1982) in the focal plane records the images of five individual Fabry-Perot fringes. Secondly, a wide-angle (all-sky) optical system is placed ahead of the Fabry-Perot etalon, to match a large field of view in the sky to the field of view of the Fabry-Perot fringes in the focal plane. In practice, about 100^{o} arc (full angle) in the sky corresponds to about 2.5^{o} arc (full angle) in the image plane, and the 100^{o} corresponds to the centre of the 5th Fabry-Perot fringe. Individual angular and radial segments of each Fabry-Perot fringes are thus coherently mapped onto the sky. Given a knowledge of the height of a specific emission layer (and assuming that the height is approximately uniform), the subsequent data analysis provides a map of line-of-sight (l-o-s) wind velocity and relative auroral intensity over the entire field of view. A subsequent data analysis stage is required to reconstitute the (assumed horizontal) vector wind field.

Figure 2 shows the schematic layout of the DIS, with the arrangement of optical components, and the light path through the instrument. The general principles of the optical system of the DIS and the necessary calibration procedures to ensure reliable and accurate data have been discussed previously in Rees and Greenaway (1983), Rees et al. (1984) and Batten et al. (1988). Many of the practical aspects of the DIS are identical to those of the UCL FPIs. However, the simplification involved in removing the scanning mirror system does introduce some complications of the calibration system in addition to those required of the FPIs, while removing one source of moving parts and inherent potential unreliability.

Briefly, the following calibrations of the DIS have to be performed:

I) Flat field sensitivity calibration, to correct for non-uniformity of optical throughput and detector sensitivity over the image plane.

II) Thermionic emission calibration, to correct for thermal electron emission, and its variation over the detector surface.

III) Full-field spectrometric calibration, using the neon 630.4 nm line, to map the base-line Optical Path Difference (OPD) variations over the image plane.

IV) Positional geometrical calibration, to map sky locations to position on the detector image plane.

V) Continuous 'spot' calibration, to monitor thermal, electronic and mechanical instrument drift.

The DIS shares the useful property of the FPI that the entire spectral pattern is recorded simultaneously. Rapid temporal fluctuations of intensity over the field of view are generally of less importance than with a spectrometer or interferometer which has to be sequentially scanned in OPD. Since the sky is imaged directly onto the photocathode of the IPD, we have always been aware that sharp spatial features and intensity gradients in the far field are imaged directly onto the Fabry-Perot fringe pattern. With the FPI, due to the small instantaneous field of view, the upper atmosphere winds invariably advect any significant airglow or auroral intensity features over the image plane within the integration period. However, for the OI 630 nm emission, such gradients are normally very small, in any event. For the DIS, with its large field of view, there is a greater potential problem caused by intensity gradients. In practice, for studies using the OI 630 nm emission, there is never a practical problem. Advective smearing due to winds, and the low spatial intensity gradients of the OI 630 nm emission always cause the intensity modulation of the fringes to be below a critical level at which wind

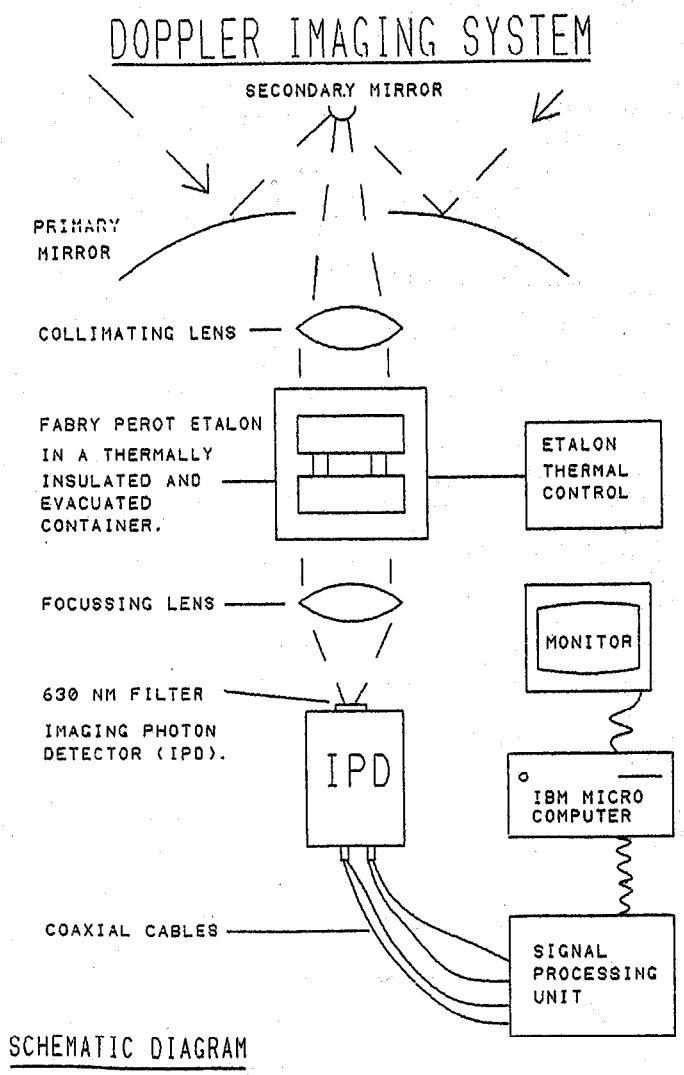

Figure 2

Figure 2: A schematic diagram of the DIS showing how the component parts are arranged within the instrument, and the path of light rays through the instrument.

errors would occur. We should, however, note that with lower thermosphere or mesospheric applications, the intensity gradients are larger, and the advective smearing is lower. Methods which have been developed at UCL to analyse DIS observations of rocket-borne shaped-charge releases (which have enormous and rapidly-changing gradients over the fringe pattern) may then have to be applied to correctly analyse and interpret the DIS fringe data.

3. Instrument Calibrations and Data Analysis:

I. The Imaging Fabry-Perot Interferometer.

The raw Fabry-Perot image data, of images of 256 by 256 pixel are accumulated into the computer memory (Figure 3). The two dimensional images, in normal operation mode, are compressed for storage, into a one dimensional array (Figure 4), comprising a radial profile - in effect the spectrum. The centre of the Fabry-Perot fringe has to be determined to the nearest pixel, before this 'reduction to radius squared' operation is performed, automatically, at the end of each integration period. Under normal observing conditions, only these one dimensional profiles and spectra are stored onto computer disk. Doppler shifts are inferred from the spectral analysis of the fringes. The radial profiles are corrected with the appropriate thermionic emission and flat-field response prior to spectral analysis.

Further corrections and calibrations may have to be applied to the radial profiles, prior to spectral analysis. Firstly, any non-linearity in the detector geometric response may be deconvolved. This correction ensures that the apparent distance, in wavelength space, between the calibration line and the zero Doppler shift of the observed auroral or airglow emission, is a constant of the instrument, rather than a possible variable. Although the instruments are, in principle, extremely stable in operation, the normal intervention of Mr. Murphy dictates that regular spectral calibration should be used to monitor changes of OPD. A neon (or other suitable gas such as Krypton) R-F excited lamp is the normal regular calibration source, with the illumination of a screen viewed by the FPI each rotation around, normally 8 discrete viewing positions. The occasional failure of a thermal control system, opening of external doors, miniscule leaks of the vacuum seal of the etalon container can thus be coped with by the regular calibrations, without any loss of data. Otherwise, it is often several months between a problem occurring and its being noted in data returned to the UK for analysis. Typically, it may be a full year before a minor problem can be fully rectified. Thus the regular calibrations provide the means of determining the health status of the instrument. Many minor problems can be corrected using the calibration data, avoiding the loss of data. Frequently, early warning signs of potential problems can be noted, improving the efficiency of planning for the infrequent but expensive visits for preventative maintenance, and sometime avoiding potentially catastrophic problems which might develop later.

The regular calibrations also allow comparison between measurements recorded with different instruments, and provide continuity between data sets obtained after minor or major changes in FPI / IPD configuration, and between instruments at different locations.

When fully corrected, each spectral profile is then analysed to determine the fringe radius, line intensity, line width and continuum intensity. There are several possible methods of analysing these spectral profiles, including that implemented by Killeen and Hays (1984) for the 12-segment multi-ring anode Image Plane Detector. Methods which have been used for peak-fitting have been reviewed by Lloyd (1984) and by Aruliah (1990). The analysis includes allowance for the calibrated instrument profile, determined periodically by a laser calibration source. This latter feature is essential for determination of temperature from the observations.

One of the most difficult factors to ascertain is the true effective baseline for wind absolute determination. Two factors need to be determined: the absolute zero velocity baseline, and its relative changes from time to time. In practical terms, it is possible to routinely and regularly determine the offset, in wavelength space, from the neon calibration lamp fringe at 630.4 nm to OI 630 nm line. For studies of the OI 557.7 nm emission, the position of a convenient fringe from a Kr calibration lamp is used to monitor relative drifts of the 'zero Doppler shift'. Other calibration lamp emission lines are available close to most of the other airglow and auroral emissions which are interesting targets for

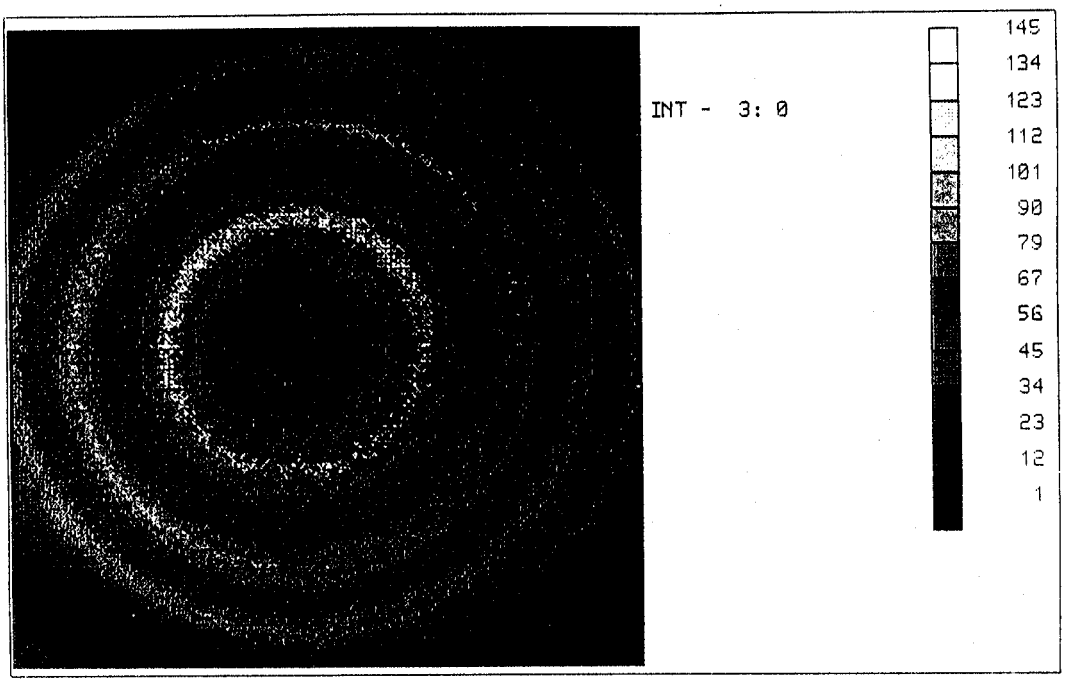

Figure 3: The raw Fabry-Perot image data, of 256 by 256 pixel, as accumulated into the computer memory.

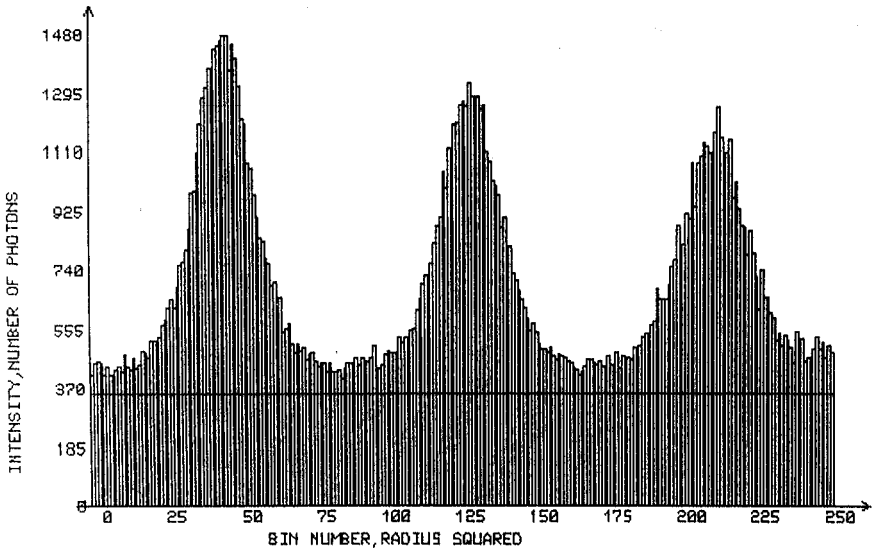

Figure 4: The two dimensional images, in normal operation mode, are compressed for storage, into a one dimensional array comprising a radial profile - in effect the spectrum.

study. The key factor is that the calibration emission can be transmitted through the interference filter used to select the atmospheric line being studied, so that there is absolutely no possible change of the spectral characteristics of the instrument from operating to calibrating mode.

Given this relatively easy method of deducing and monitoring relative drift, the more difficult problem of determining the absolute zero velocity baseline has to be faced.

The normal method is to use all available and valid zenith observations taken over an extended period (several months) of observations, corrected for relative drifts by using the R-F excited spectral lamp calibrations. The usual assumption is made that, when averaged over a long time period, the mean vertical wind would be small, almost certainly less than 10 ms^{-1}. Much larger vertical winds occur for relatively short periods, and particularly at the high latitude stations (Rees et al., 1984a,b). The validity of this assumption has to be cross-checked each night by ensuring that the zenith Doppler shift lay midway between the mean Doppler shifts obtained from opposing cardinal directions. In short, establishing that the instrument, data and data analysis methods are all working reasonably, the long-term base-line can be established to within 10 ms^{-1}. Given this base-line, relative changes are then monitored using the R-F calibration source. In principle, a convenient laboratory source of the OI 630 nm line would remove some residual ambiguity, and such sources have been demonstrated to operate for a moderate lifetime. However, the R-F lamps have a very long lifetime and are both cheap and reliable, and are also very easy to replace within the instrument. Those sources of OI 630 nm emission which have been demonstrated still have some drawbacks in terms of limited lifetime and a need, because of relatively low intensity, to arrange a very efficient optical illumination system into the interferometer. Regrettably, this would involve considerable re-design and engineering of the present existing instruments.

There are several methods of presenting the data obtained from individual measurements of the Doppler shift obtained in the series of directions. Firstly, neglecting the vertical wind (which can be, and usually is observed, but only directly overhead the observing station), the line-of-sight wind component can be converted into an equivalent horizontal wind component. The sequence of wind components obtained in successive directions can then be used either independently, or alternatively, they may be combined. For example, the mean horizontal wind flow can be estimated from the least squares fit of a cosine to observations of the six cardinal, line-of-sight, Doppler shifts. It is then possible to analyse for a linear gradient in the wind flow. The FPI observing circle is normally relatively large, spanning some 4^{o} - 8^{o} of latitude, depending on the zenith distance observed, and the altitude of the emission layer. Values for the individual wind components, related to their well-separated locations around the 'observing circle', plus the mean wind and linear gradient can be tabulated either 'as obtained', or alternatively at 15 minute intervals by linearly interpolating between individual data points. It should be noted that the mean wind is relatively insensitive to any error in the point of zero Doppler shift as it mostly depends upon the difference between Doppler shifts from opposing directions. At high latitude stations in the auroral oval or polar cap, the gradients and temporal changes of winds are often very large, particularly under disturbed geomagnetic conditions. The mean winds have then to be referred back to the 'absolute zero velocity baseline'. Frequently, for detailed interpretation, for example comparison with model simulations, only the independent wind components are directly useful for other than statistical analysis.

Under some conditions, a calibrated photometer has been located alongside the FPI to provide direct calibration of the FPI line and continuum intensity measurements. Under these conditions, the FPI line intensities have been converted to an equivalent zenith intensity (i.e. Lloyd et al., 1989). More usually, an all-sky camera is run along-side (normally part of the standard instrumentation at sites such as IRF, Kiruna). These all-sky data provide the necessary monitor of poor or variable observing conditions. A meridian-scanning photometer has also been used from time to time to provide a means of cross-calibrating the overall sensitivity of the Imaging FPI.

All Fabry-Perot wind measurements are susceptible to corruption from atmospheric scattering due to aerosols and clouds. Normally, the entire data set is inspected to locate periods when scattering may have been significant. Scattering, by any mechanism, is usually characterized by a reduced mean Doppler wind and may be accompanied by large and sudden apparent wind gradients and changes, as

for example if a patch of cloud suddenly moves into the field of view. Under very cloudy conditions, the Doppler shifts and thus 'winds' measured in all directions normally fall to very low values, and there is an accompanying reduction in fringe contrast which almost uniquely identifies the period of next to useless data. Conversely, the detection of a large mean wind with small gradients implies that scattering is probably insignificant. Clouds are an obvious source of scattering, but low altitude aerosols [Abreu et al., 1983], local atmospheric pollution and the observing dome are other potential scattering sources. Clearly, in studying many phenomena, long-term, unattended observation is essential, and it is quite impractical and prohibitively expensive to always have an operator in attendance merely to record sky and viewing conditions. Paradoxically, light pollution from nearby cities creates the fringe contrast reduction which usually paints marginal or variable conditions in an unambiguous way.

The effects of tropospheric scattering are most severe when there are large intensity gradients across the FPI observing region in the sky. This is often the case during periods of strong auroral activity. Results taken during such periods do occasionally, display the characteristic signature of scattering, as for example simulated by Abreu et al. (1983) and thus may have been contaminated. Generally, such periods have been excluded from the final data set. This is particularly important with long-term studies, and with statistical analyses using data from extended periods.

The instruments are normally attended for approximately 1 month, each instrument, each year, when it is possible to fully characterise the instrument, the data, and the response to specific meteorological conditions. These periods of attendance have been used to build up an extended data base of information relating data quality to observing conditions (and to particular airglow and auroral activity). This data base from observations with an operator in attendance amounts to approximately 10 % of the total data, or at least 300 nights out of the total of more than 2000 nights of useful data, and is the basis for selection of nights, observing directions and observing periods when the data is believed to be of adequate quality for analysis and interpretation.

II. The Doppler Imaging System.

The Doppler Imaging system shares much common hardware and software with the Imaging Fabry-Perot interferometer. It is not surprising, therefore, that the calibration procedures (tabulated earlier) and the data software also have a common body of methods and analytical routines.

Figure 5 shows a full two-dimensional image of the sky obtained by the DIS during a period of moderately active auroral conditions at 06:13 UT on 27th November 1987. This image is the raw data obtained by the DIS. North is directed upward, east to the right. In the southern part of the image, part of a distinct second set of fringes can be seen. These are from a neon calibration lamp (630.4 nm), illuminating a calibration 'patch' on the plexiglass dome covering the DIS. There is a dark area in the centre of the image. This is the shadow of the secondary mirror holder. The three dark spokes in the image are the out-of-focus silhouette of the secondary mirror spider mount. The central shadow masks the first FP fringe, while the outermost fringe is incomplete and partly vignetted, and cannot normally be used in the wind analysis.

The first stage in the analysis of the DIS data is the real-time reduction of the full 2-D images to 24 spectral profiles. The photon counts in 24 equal area sectors, each of 15° arc, are reduced to a linear wavelength presentation, based on the centre of the Fabry-Perot fringe pattern. This process is exactly equivalent to that shown in Figure 4 in respect of the Imaging FPI. An example of this reduction is illustrated in Figure 5 of Batten et al. (1988). The centre of the fringe pattern must be accurately determined before any reduction takes place - this is a process which is performed, usually by iteration, using a spectrum obtained from the R-F excited neon calibration lamp. The 24 spectral profiles - 'reduced to radius squared' - due to the quadratic relationship between radial location and wavelength in the image plane, are then analysed a-postiori to provide:

(i) fringe peak locations with error estimates,
(ii) a map of the intensity of the OI 630.0 nm emission (96 elements), and
(iii) a map of the background sky intensity (96 elements).

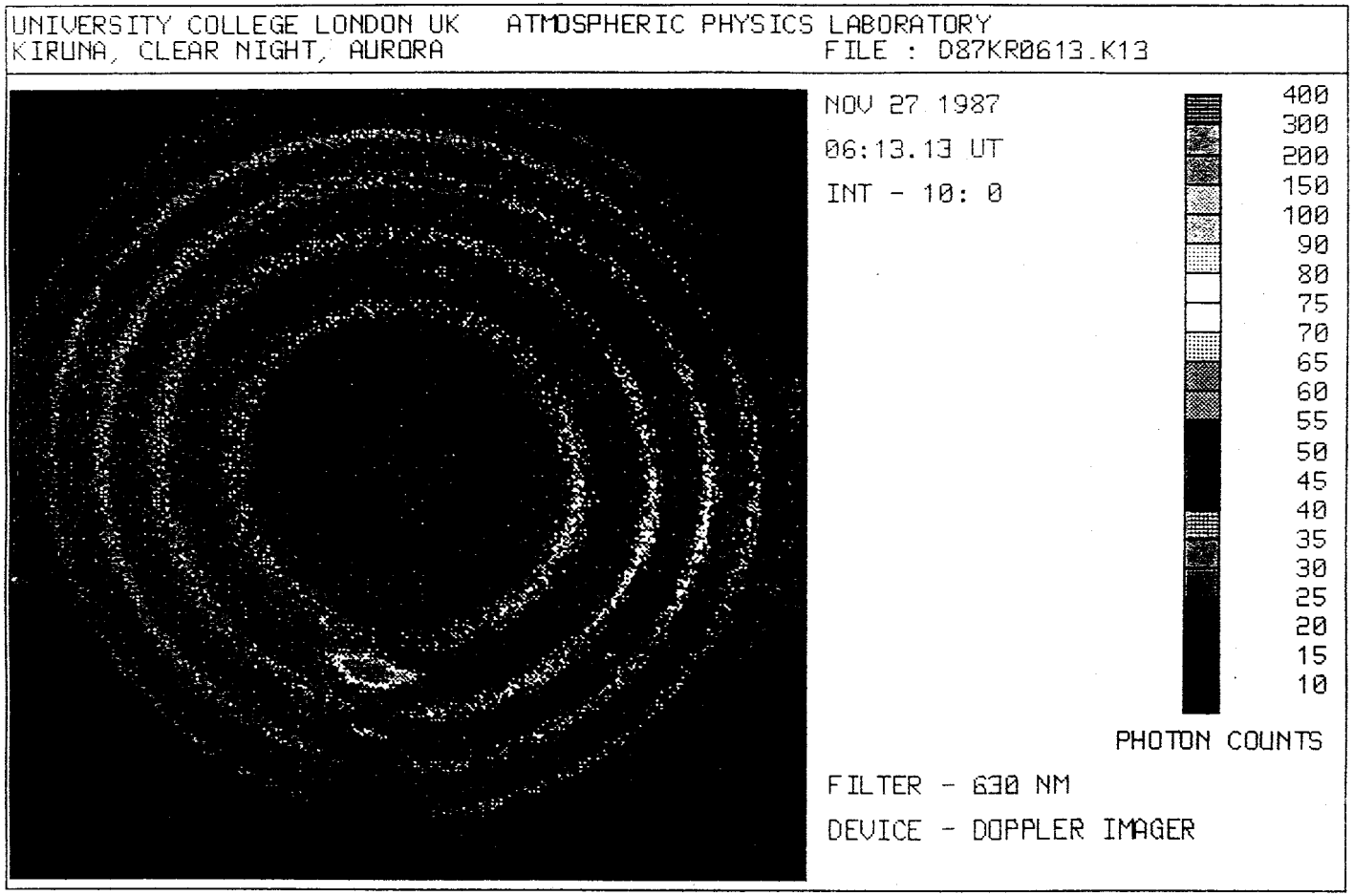

Figure 5: A full two-dimensional image of the sky obtained by the DIS under conditions of moderately active auroral activity at 06.13 UT on 27th November 1987. North is at the top, east to the right.

After the locations of each of the spectral peaks are determined, the Doppler shifts can then be calculated, and the l-o-s wind velocities over the field of view can be deduced, based on the calibration data, and on a determination of the 'zero velocity' fringe positions. The 'zero velocity' fringe determination has to be based on the analysis of a considerable body of real data, since it is not practical to routinely operate a source of the OI red line at remote field locations. The principle is fundamentally similar to that used for more traditional ground-based FPIs. The analysis of the DIS data to this stage has been fully discussed in Batten et al. (1988).

The absolute line-of-sight wind velocity component (v) is calculated from:

$$v = c \cdot \lambda / 2t \cdot (cal - dat) / fsr$$

where:

- c = velocity of light in vacuum
- λ = wavelength of the emission
- t = the etalon gap
- cal = position of the calibration peak
- dat = position of the data spectral peak after instrument corrections
- fsr = free spectral range (adjacent peak positions)

Each typical DIS image is reduced to twenty four 15^0 sectors, each containing four complete fringes which can be fully analysed. This generates 96 individual measurements of the radial l-o-s wind velocity for each integration period. The integration period is usually chosen to be ten minutes, giving six images, and 576 individual l-o-s wind measurements per hour.

4. Vector wind determination for the DIS.

The 96 individual l-o-s wind components are reduced to equivalent horizontal (and radial) wind components by the simple assumption of a zero vertical wind component. The vertical wind directly over Kiruna is monitored by means of the co-located FPI. The RMS vertical wind is normally less than 10 ms^{-1}, however, on occasions, much larger vertical winds do occur (Rees et al., 1984a,b). The assumption of zero vertical wind over the entire field of view of the DIS may, obviously, introduce a significant error under some conditions. The 96 measurements of the horizontal wind component, radial to Kiruna, are then analysed by a maximum entropy method, to calculate the mean wind field.

To produce a unified vector wind field, a continuity condition must be assumed, effectively coupling the data from adjacent azimuthal, radial, and temporal elements of the derived wind patterns. The question of how best to derive the maximum information on the horizontal wind field has to be addressed. There are localized structures within the field, and all the azimuthal, radial, and temporal information available from the individual, and sequential, Doppler images has to be used. A strong wind observed at one location, at one azimuth, should have corresponding features at adjacent azimuth angles, in adjacent fringes, and in consecutive images. It is therefore assumed that the vector wind field is a single valued, continuous, function and that it can be described by a two-dimensional polynomial. It is further assumed that the vector components can each be represented by two orthogonal components and that these components can be described by perpendicular polynomials.

At this stage it is possible to set up the least squares criterion:

$$\chi^2 = \sum_{i=1}^{np} [\, V(r,\theta) - M(r,\theta) \cos[\theta - \phi(r,\theta)] \,]^2 / \sigma^2 \qquad [1]$$

A Fourier low-pass filter is used to smooth the azimuthal components and to interpolate between missing data points. Weighted Chebyshev interpolation is then used to calculate the vector component of the field in all of the twelve measured, radial, cross-field directions.

The wind vector is described by the equation:

$$W = V \cos(\theta - \psi) \qquad [2]$$

where:

W = line-of-sight wind velocity
V = wind velocity
θ = observing direction
ψ = bearing of wind vector

$$\Rightarrow \quad W = V \cos\theta . \cos\psi + V \sin\theta . \sin\psi \qquad [3]$$

The first harmonic of the Fourier transform is:

$$W = A \cos\theta + B \sin\theta \qquad [4]$$

Therefore, the harmonics A and B can be equated to the average wind velocity V and Bearing ψ by:

$$A = V \cos\psi \quad \text{and} \quad B = V \sin\psi \qquad [5]$$

The direction and amplitude of the true vector (of which A and B are the orthonormal components) can be calculated at each point.

The true wind direction is given by $\psi = \text{Arctan}(B/A)$, and the wind velocity amplitude by $(A^2+B^2)^{1/2}$. Each component of the vector wind field has thus been estimated from all the available l-o-s data, weighted for distance from the point in question. The set of all the individual wind vectors can be plotted to show the structure of the wind field at an altitude assumed to be 240 km. With the given geometry of the all-sky optics of the DIS, this corresponds to a circle of approximate radius of 240 km, centred directly above the Kiruna. The deduced horizontal wind pattern contains the maximum amount of valid spatial information available within each Doppler image, consistent with the quality of the available data. The data quality varies within each image and from image to image, mainly as a function of the localised emission rate for O^{1D}. The χ^2 criteria is observed to decrease steadily as the number of Fourier and polynomial components is increased, until it settles down to a fairly constant value χ_0^2. Once a steady value is reached, this indicates that the closest approximation justified by the data quality has been achieved. If the degree is too high, the value of χ^2 decreases again. This indicates that the data is being over-fitted, and that noise is being included. The order of smoothing also takes account of a maximum entropy constraint.

The maximum entropy method (MEM) is a powerful theoretical approach to the problem of selecting one of a choice of several, otherwise equally valid, solutions to a data set, making the least number of assumptions about unmeasured parameters (Burch et al., 1983; Gull and Daniell 1978; Gull and Skilling 1984; Skilling and Bryan 1984; Sibisi 1983). The maximum entropy method always selects the smoothest solution, i.e. that solution which includes the minimum structure consistent with the data. The entropy, S, is calculated for the magnitudes of the resulting wind fields for different orders of polynomial and Fourier smoothing.

$$\text{Entropy, } S = -\sum_{i=1}^{n} p_i \log p_i \quad \text{where} \quad p_i = f_i / \Sigma f_i \qquad [6]$$

where f_1 to f_N are a set of numbers, in this case those relating to the wind fields. The chosen orders of smoothing were those which gave the maximum entropy consistent with the constraint of χ^2 approximately equal to χ_0^2.

Figure 6 displays a series of full images of the Doppler horizontal wind components directly derived from the line-of-sight measurements, data obtained between 20.33 UT and 21.38 UT, 25th January 1988. It is only the directly-measured line-of-sight component which is used in this analysis stage, with the calculation of the component of the assumed horizontal wind from the measured l-o-s component. It can be seen that the 'winds' are entirely convergent / divergent - an artifact which is totally unrealistic. The OI 630 nm intensity patterns are displayed as the background scalars / intensity values.

There should be continuity between successive Doppler images. Within the disturbed auroral oval, accelerations of the thermospheric wind can be very large at times. However, within a given gas parcel, only a finite wind velocity change can occur within the ten minute interval between successive images.

Using the analysis method described for deriving the vector wind components from the measured l-o-s components, the corresponding wind vector patterns are displayed in Figure 7. The vector wind patterns, derived from the measured l-o-s components by fitting for the unmeasured radial wind components, as described earlier, appear as a much more realistic fluid flow pattern. These images were obtained at intervals of ten minutes on this night of moderately disturbed auroral and geomagnetic activity. The sector at 180^{o} azimuth contains no measured wind or intensity information, due to the calibration patch (Figure 5). The wind vectors have, however, been interpolated across this calibration sector by the analysis / fitting process. Between 20:55 and 21:18 UT, there is a general surge in the southwestward wind velocity, particularly noticeable in the southern part of the field of view. This corresponds to the auroral brightening in the southeast part of the field of view of the DIS. In the same period, the winds in the northern part of the field of view slightly decrease, indicating a significant wind acceleration as the thermospheric wind flow crosses the arc. At this stage, it is not possible to determine whether ion drag or the Joule heating associated with the arc play the larger role in the observed wind changes.

There are several inherent problems in the study of small scale wind velocity structures.

(i) Small cloud patches:

Small patches of cloud can cause scattering of the 630.0 nm radiation in a part of the field of view, giving anomalous results, while not warranting the identification or rejection of the whole hourly period as cloudy. Clouds usually produce a localized region of anomalously low wind velocities. This is, usually and fortunately, accompanied by a localised decrease in intensity. The presence of cloud above Kiruna is routinely recorded by an all-sky camera (16 mm colour film). These data are analysed to provide a tabulated hourly average of auroral intensity and weather conditions, published in the Kiruna geophysical data summary on a three monthly basis. Caution is obviously necessary when interpreting data obtained during periods of partial cloud cover, and a review of the all-sky camera film is usually used to verify conditions during periods of specific interest. No data from partly cloudy periods has been included in this present analysis.

(ii) Vertical winds

Vertical winds can further complicate the analysis. The DIS would interpret a uniform upward motion as a divergent wind field. A uniform downward motion would, conversely, appear as a convergent wind field. As yet, no systematic account is made of the possible existence of vertical winds in the analysis of the DIS data. Vertical winds generally have relatively small values compared with the horizontal wind velocities. At times, however, vertical winds of more than 100 ms^{-1} have been observed (Rees et al., 1984a,b). The vertical wind directly over Kiruna is measured routinely by the co-located FPI, however, these local observations are certainly unlikely to be valid for the entire region observed by the DIS.

(iii) Advective Smearing

A parcel of gas moving at 100 ms^{-1} travels 60 km during the typical ten minute integration time used by the DIS. For such an average wind velocity, structures smaller than 60 km scale size will be partly

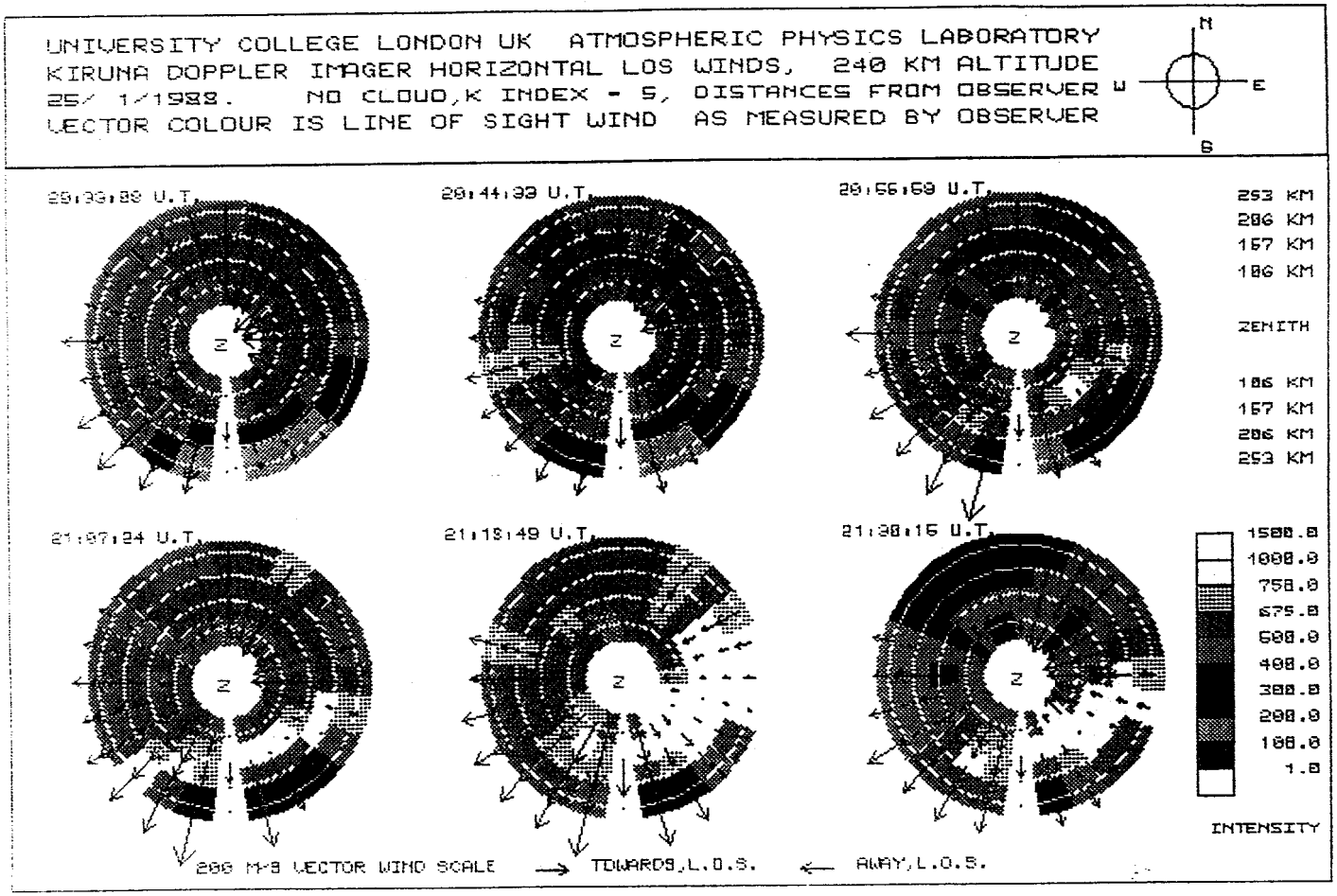

Figure 6: A series of full images are shown of the line-of-sight Doppler shifts, converted into equivalent horizontal wind components obtained between 20.33 UT and 21.38 UT, 25th January 1988.

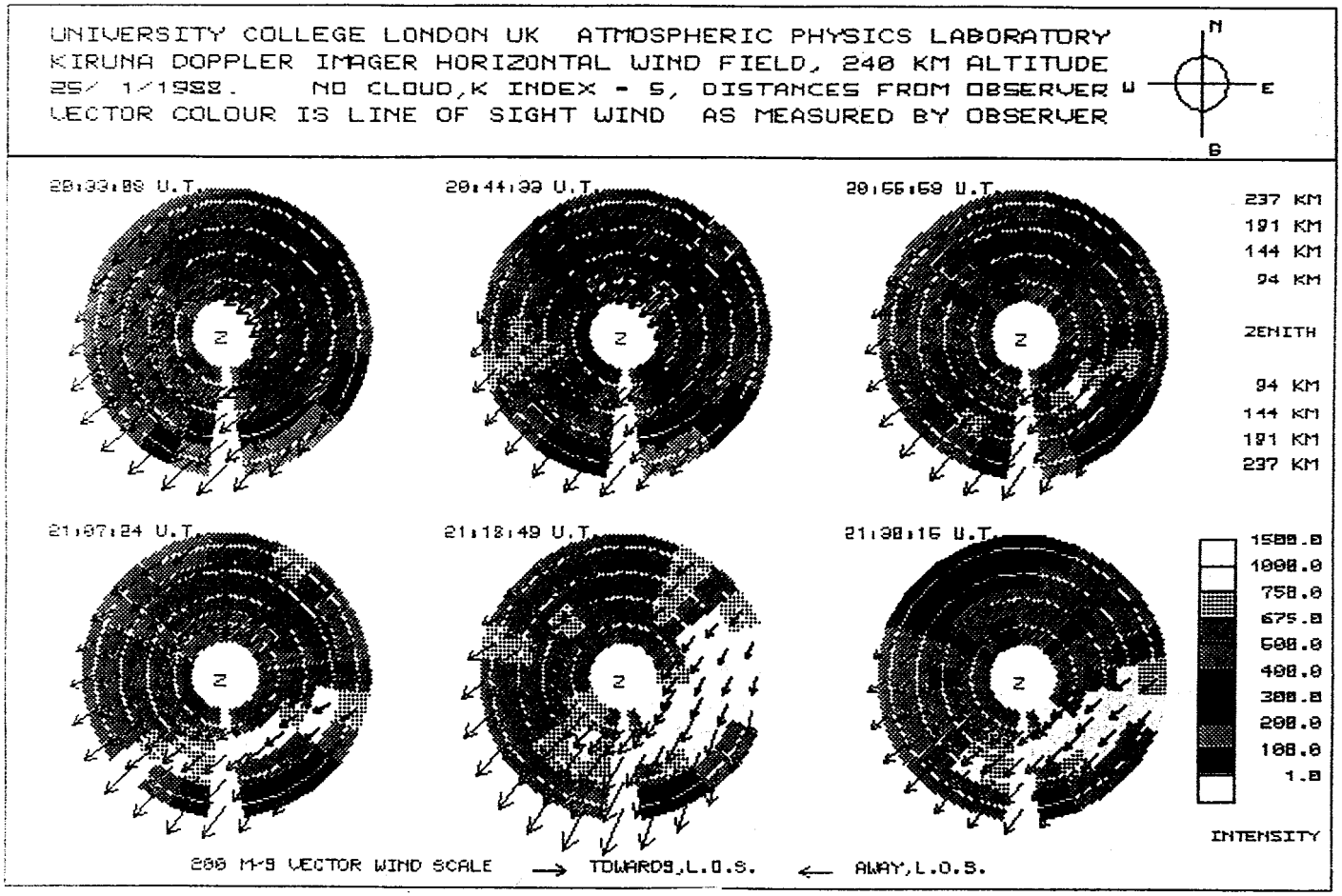

Figure 7: The horizontal vector wind patterns, corresponding to the MEM fitting to the line of sight wind components shown in Figure 6, are displayed.

smeared. The degree of smearing increases with wind velocity: for a 300 ms^{-1} average wind velocity, any structures smaller than 180 km will be partly smeared during a ten minute integration period.

(iv) The maximum entropy technique

The maximum entropy technique, employed to fit the individual l-o-s wind velocity vectors, itself introduces further smoothing. The structures discernible in the data thus tend to have scale sizes significantly larger than the minimum which may actually occur in the thermosphere.

Practical Solutions

Solutions to these problems mainly involve experience with the data handling and common sense. In principle, advective smearing can be reduced by decreasing the integration time. However, during periods of low intensity several successive images would have to be processed to obtain a sufficiently high signal to noise ratio. This solution is thus partly limited by signal levels and detector sensitivity, and partly by the logistics of data storage. Using a ten minute integration time, the DIS currently stores more than a megabyte of data per night. Shorter integration times would require larger magnetic or optical disk storage facilities, both of which are now realisable, but have not yet been implemented. Improvements in the signal to noise ratio can also now be obtained using IPDs with Gallium Arsenide photocathodes. It is hoped to be able to operate the DIS at IRF, Kiruna, with such a device during the 1989 / 1990 winter.

The problems of partial cloud cover and vertical winds require a careful assessment of the available additional information from the all-sky camera and the co-located FPI. Inevitably, the result is that some perfectly valid data is rejected along with data which is certainly contaminated either by local cloud scattering or by localised regions of high vertical winds.

The data shown in Figure 7 (Jan 25, 1988) illustrate the problem of advective smearing. The wind vectors displayed are of the order of 250 to 300 ms^{-1}. There is little discernible small scale structure in the images, and the wind flow appears uniform over the whole period displayed. At 21.18 UT there is an enhancement of the wind flow in the southwest of the image and a general anticlockwise rotation in the eastern half of the field of view. Both of these features could perhaps be related to the enhancement of 630.0 nm emission which started at 21:07 UT, and continued through 21:38 UT.

For lower wind velocities, i.e. less than 100 ms^{-1}, the smearing effect is not so significant and smaller scale structures can generally be seen. However, for low wind velocities, the errors on the individual measurements constitute a larger proportional error than for higher wind velocities.

5. Analysis of Temperature data.

The general principle of temperature measurement with the imaging FPI and DIS systems is identical to that of the conventional FPI (Hernandez, 1986, Meriwether, 1990). The instrument spectral / line profile has to be derived with adequate accuracy, and deconvolved from the observed line profile. This process is included in the routine analysis process for the Imaging FPI and for the DIS. Because of the way in which a number of fringes are compressed onto the imaging detector of the DIS, it is inherently less capable of determining accurate temperatures than is the Imaging FPI. Since, at present all of the Imaging FPIs use high resolution etalons without a facility for scanning the OPD, the process of calibrating the line profile is somewhat more complex than for the conventional FPI, since each part of the free spectral range has to be calibrated for its instrument function. The calibration fringe and the OI 630 nm fringe , for example, rarely overlap in the image plane. This means that an ad-hoc arrangement for pressure scanning has to be introduced to obtain an initial sequence of instrument profile calibrations of the entire detector, before the instrument can be settled into a mode where, by use of a single mode stable laser, any minor changes can be monitored regularly.

We should, however, note that with the Imaging FPI and DIS, there is an important practical aspect, relating to the remote location and automatic operation of all of the FPI instruments of this class. The R-F excited neon lamps are very stable sources of wavelength calibration, and have excellent reliability.

However, they provide a relatively broad spectral line (corresponding to, typically, 700 - 900K). They also do not have a particularly stable line width, since this is dependent on the operating conditions. Single-mode stabilised He-Ne lasers certainly can be used to derive the instrument function with adequate accuracy but are, however, still relatively expensive and unreliable for long-term operations of a remote automated system. Only one of the present Imaging FPI systems (Bear Lake, Hardware Ranch, Utah State University) currently has such a stable laser incorporated into the system for routine calibrations of the instrument profile. This is the only Imaging FPI facility which presently makes routine temperature measurements in addition to the wind flow observations. For some special studies, particular efforts have been made to derive an effective instrument profile from calibrations with an unstabilised laser. Some results comparing thermospheric temperature measurements from the FPI at IRF, Kiruna, and ion temperature measurements from the EISCAT radar were, for example, published by Rees et al (1984c).

6. The Instruments and their Typical Results.

The Imaging Fabry-Perot Interferometers and DIS: Stations, Observing Periods and Data.

The Imaging FPI instruments which have been built at UCL, their locations and normal operational modes, are summarised in this section. These instruments, with the exception of the FPI at Halstead UK, are all operated by the local cooperating research institute. The Halley Bay instrument belongs to the British Antarctic Survey, while that at Saskatoon belongs to the Institute for Space and Atmospheric Studies, University of Saskatchewan, Saskatoon. The following section provides a little more information on each station and instrument. More information, and the detailed scientific results obtained from each of these instruments and stations, can be found in the appropriate references.

Kiruna, Sweden: (67.8^{o}N, 21.2^{o}E)

Since the 1980 / 81 winter, at least one of the imaging FPIs has been operated during the winter period at the Institutet RymdFysik, Kiruna, and since the 1981 / 1982 winter, one or more instruments have been maintained in continuous automatic operation.

At present, there are three imaging FPIs in routine operation at IRF, as well as a Doppler Imaging System. Two of the FPIs are single-etalon instruments, currently making routine observations of the OI red and green line emissions. Another FPI is a triple-etalon system. This instrument is still in a process of development for daytime / year-round thermospheric wind measurements of OI 630 nm. The instrument is based on the hardware used for the UCL high altitude balloon flights (Rees 1985) where its target has been to measure stratospheric wind in daytime by observing the Doppler shifts of absorption lines due to molecular oxygen and water vapour. The triple-etalon system has been used for a series of developmental tests of the triple-etalon imaging FPI concept. It is, however, an expensive and relatively complex instrument. During the 1987 / 1988 period, it was run for 12 months continuously. It is expected that in late 1989 or early 1990, the instrument will be further upgraded with two new high-performance capacitance-stabilised etalons, and with a new 32-channel, multi-element anode detector recently obtained from ITT.

Some 40 papers have been published which have involved the results obtained from the UCL FPIs at Kiruna, including the use of their data in conjunction with large-scale observations from Dynamics Explorer, the global network of Fabry-Perot interferometers and incoherent scatter radars (such as within the SCOSTEP WITS and GITCAD / LTCS programmes). There have also been a number of studies using combined data sets from the nearby EISCAT radar facility.

Figures 8 and 9 show some particularly interesting storm-time results from the peak of the last solar cycle. In Figure 8, the behaviour of the thermospheric wind in the afternoon hours during a disturbed period is highlighted (Dec. 12, 1981). Between 14 and 16 UT, the westward (sunward) winds, excited initially by ion drag within the expanded auroral oval, reached speeds in excess of 900 ms^{-1}. This situation has been discussed in some detail by Fuller-Rowell and Rees (1984), and corresponds to resonant flow within the dusk auroral oval and polar cap regions. In Figure 9, the comparable situation

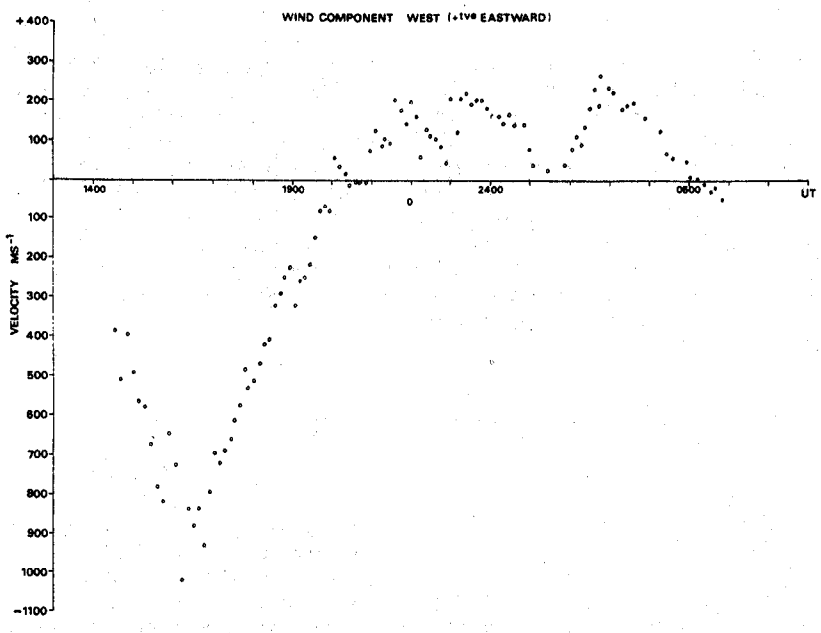

Figure 8: The response of the zonal component of the thermospheric wind at Kiruna during a disturbed period 14 - 19 UT on Dec. 12, 1981.

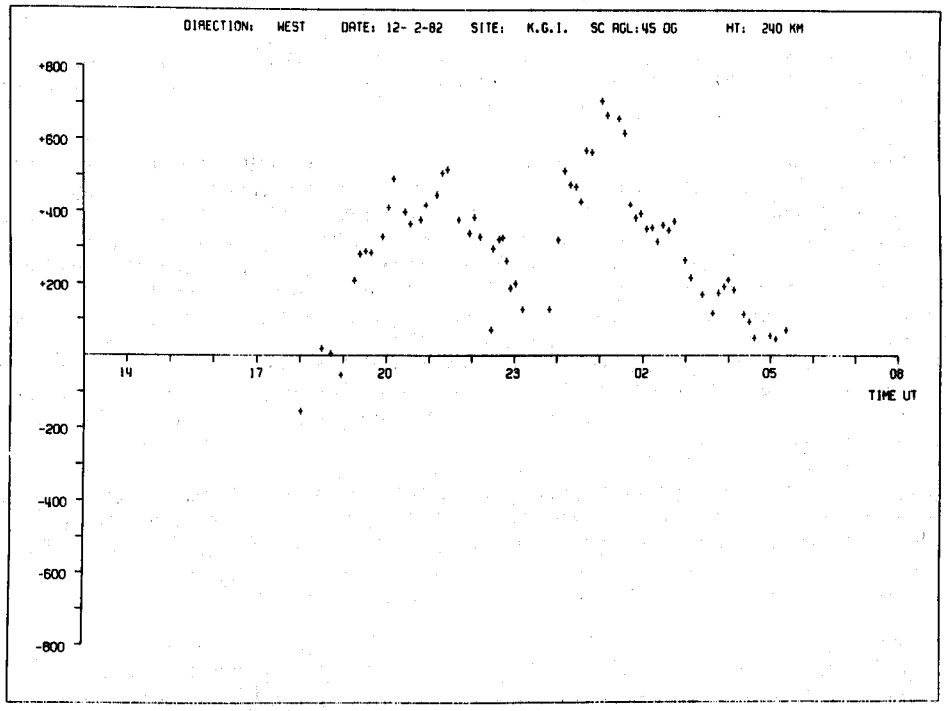

Figure 9: The response of the zonal component of the thermospheric wind at Kiruna during a disturbed period 19 - 03 UT on Feb. 12/13, 1982.

in the dawn auroral oval is shown. Normally, in this region, it is quite difficult to generate very strong sunward winds via ion drag. Feb. 12 1982 was, however, an unusually disturbed period, with the total IMF reaching 40nT. In addition, there was a strong negative IMF BY component (Rees et al, 1986). This condition strongly enhances ion flow in the dawn auroral oval, and leads to a situation where the eastward (sunward) wind components peaking at approximately 700 ms^{-1} could be generated and maintained for several hours. There were also extreme (500 - 600 ms^{-1}) southward winds during this unusual period. This particular disturbed period continued for approximately 4 days.

More than 1000 nights of high quality data are available, obtained during clear sky conditions, from the Kiruna instruments. The statistical analysis of these data have been presented and discussed by Lloyd (1985), Rees et al. (1985, 1987) and by Aruliah et al. (1989).

Halstead, England: (0.1°E, 51.3°N)

The instrument operated here is the 'home base' (literally in the 'back yard' of D.R.). Given the famous average UK weather, this station is generally used for development and testing work, shaking out the variety of bugs in new instruments before they are dispersed, unattended, to the far parts of the world. The instruments which are set up from time to time are also used for training purposes, to reduce the initial problems associated with encounters between students and relatively inexperienced or new staff and the instruments. Various problems which occur in instruments in remote places can sometimes be duplicated, and occasionally solved by attempting solutions on a local instrument, otherwise nearly identical to the instruments out in the field. In 1981-1983, the effects of several large geomagnetic disturbances were recorded. The data obtained under these conditions were qualitatively similar to those discussed later under Utah State University Instrument. Similarly, at the present time, 1989, two large disturbances (March 1989, Sept. 1989) have been observed.

Halley Bay, Antarctica: (75.5°S, 26.8°W, L = 4.2)

This instrument was built in 1981/82 for a collaboration between Dr. R.W Smith (then at Ulster Polytechnic), the British Antarctic Survey (Dr. Alan Rodger, BAS, Madingley Road, Cambridge, UK) and UCL. The instrument has been in regular operation at the BAS station at Halley Bay in the Austral Winter months most years since then. It is by far the most remote of the Imaging FPIs in this group, and requires a greater amount of instrumentation back-up than any other system, to overcome the various problems. Very low humidity, and the once-per-annum visit which is possible for significant re-supply and major maintenance are among the greatest problems. Nevertheless, the instrument has run reliably for most of the period after the first couple of observing winters. The instrument provided the first southern polar observations of thermospheric winds from a ground-based FPI. Until very recently, the only other south polar thermospheric wind available was that from the DE-2 satellite-borne FPI.

Figures 10 and 11 show some typical results from the Halley Bay instrument in the 1987 austral winter, which are discussed in detail by Stewart et al (1985). In Figure 10, the winds from a relatively disturbed day (12 / 13 July 1983) are shown, compared with a global numerical model simulation. In the early morning hours, equatorward winds reach 200 m/sec, very similar to values in the model, although the observed winds between 08 and 10 UT differ significantly from the model prediction of a continued equatorward component. In Figure 11, the wind response observed on a quiet day (July 15 / 16 1983) are shown. In this case, the maximum equatorward winds are significantly lower in the period from midnight to 06 UT. Other results have been presented by Stewart et al. (1988).

Svalbard, (Initially at Nye Alesund, later at Longyearbyen): (78.2°N, 15.6°E)

UCL have operated, in collaboration with the University of Tromso (Dr. Kjell Hendricksen), one of the FPIs at a station in Svalbard since 1983/4. Again, the remote nature of the site and the low humidity have created operational problems which needed to be overcome before reliable operation could be maintained. Since 1985, the station has operated most of the time during most winters, however, it is the least attended and supervised of any of the UCL instruments, so that even the slightest problem can cause a partial or complete loss of data.

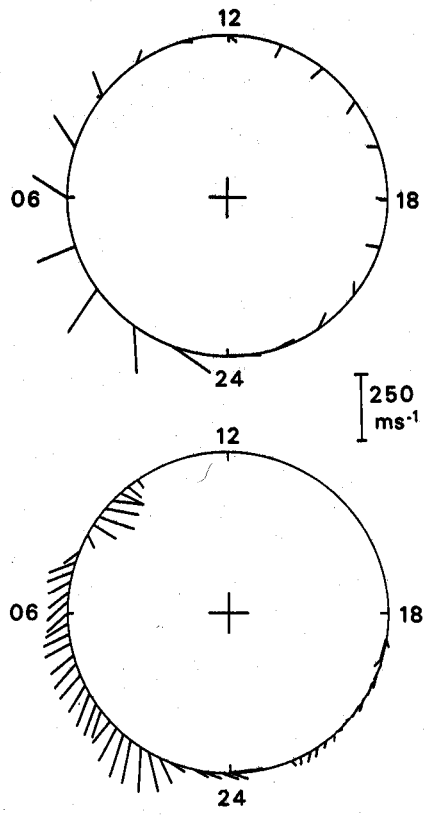

Figure 10: Thermospheric wind data from the Halley Bay instrument in the 1987 austral winter. July 12 /13 1983 was a disturbed day, with Kp varying between 3+ and 5, and with prolonged local magnetic activity. The predicted winds from a model simulation (UCL / Sheffield Model) are in the upper segment, while the observed winds are in the lower segment.

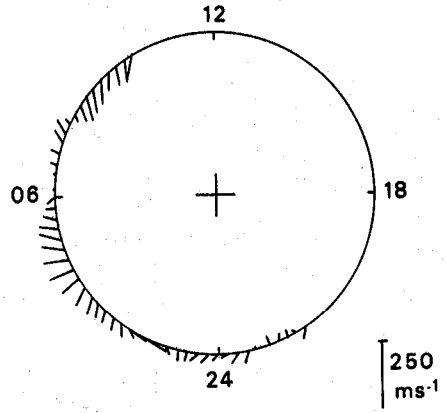

Figure 11: Thermospheric wind data from the Halley Bay instrument in the 1987 austral winter. July 15 / 16 1983 was a geomagnetically quiet day.

In conjunction with the data from the conventional FPI operated there by the University of Alaska (Dr. R.W. Smith), thermospheric wind data is available from Svalbard for most of the last solar cycle. The station shares an advantage with a few other stations: during the midwinter period, the instrument can operate for some two months on a continuous basis, in a period when the sun is always more than 6 degrees below the horizon. There is a distinct advantage in obtaining 24 hours (and sometimes several days) of continuous, unbroken, data about thermospheric circulation. This is of great advantage in comparisons with model predictions, and provides continuity of phenomena and particular events which is often lost when the lower-latitude instruments switch on or off in the middle of interesting events.

Some typical results from the Svalbard instrument are shown in Figures 12 and 13, representing relatively quiet, and very disturbed geomagnetic conditions, respectively. On the quiet day, 27 December, 1987, the wind magnitudes are less than 200 ms^{-1}, with a general pattern corresponding to a flow directed anti-sunward. On February 12, 1988, as the result of the strong geomagnetic activity, the winds are generally 300 - 500 ms^{-1}. In the midnight period, the winds are strongly equatorward (300 - 500 ms^{-1}), while the zonal component changes from eastward before UT midnight to westward after UT midnight. Typical zonal velocities on this day are 300 - 400 ms^{-1}. Again the flow is that within the geomagnetic polar cap, the strong flows responding mainly to ion drag forcing within the disturbed auroral oval, in response to disturbances in the solar wind and a large (80-100 Kv) cross-polar cap electric potential.

Kilpisjarvi: (68°N, 21°E)

Since 1982 / 1983 winter, a 15 cm instrument has been operated at Kilpisjarvi, Finland, in collaboration with the Finnish Meteorological Institute (Dr. Risto Pellinen, Helskinki, and Sodankylia Observatory). The instrument is located at the home of the late Mr. Harinkowski, whose enthusiasm and continual support were the mainstay of the operation at Kilpisjarvi for many years.

The instrument is relatively remote from the point of view of maintenance, however, the instrument operations are regularly supervised, so that minor problems (full data disks, snow on the dome etc) are noted and solved rapidly. The instrument has been used to monitor the OI red line 630 nm most of the time. At that location, it is a little more in the 'centroid' of the EISCAT observing region, and also of the STARE radar system. Additionally, given the local variations of weather during the Scandinavian winter period, a second site, although only 160 km north of Kiruna, is of great assistance in providing continuity, some data cross-check, and extending the periods of joint observations, as with EISCAT, when detailed studies of thermosphere-ionosphere interactions can be studied.

Occasionally, the thermospheric wind data from Kilpisjarvi are available when all three of the northern European stations are clear. Under those conditions, the combination of the data from all three stations provide a very interesting insight into the behaviour of thermospheric flows under various geomagnetic activity conditions, and through the dusk, midnight and dawn periods. Three examples of data obtained under such conditions are shown in Figures 14, 15 and 16. The continuity of thermospheric wind flow between the three stations is quite clear. In Figure 14, the flow reversal occurs between Svalbard and Kilpisjarvi during the afternoon hours 15 to 20 UT. In the midnight period (20 to 02 UT), there is a continuous flow over the polar cap, into the auroral oval stations, with some divergence of the flow to the south of the Kiruna station. In the early morning hours, there are strong southwestward winds observed at Svalbard, but these flows do not reach Kilpisjarvi and Kiruna, where the flow becomes changeable around the dawn period. These data were obtained during relatively quiet to moderately disturbed conditions.

In Figure 15, the winds observed at Svalbard are very strongly eastward during the period from 18 to 23 UT. The wind flow early in this period at Kilpisjarvi and Kiruna is relatively weak and changeable, but becomes southeastward after 18 UT. There is no clear flow reversal between Svalbard and Kilpisjarvi on this night. During the midnight hours there is a lack of flow continuity between Svalbard and the other stations, and again the flow patterns are variable during the dawn period, when the auroral oval passes poleward of Kiruna and Kilpisjarvi. The overall flow distribution during this period was quite

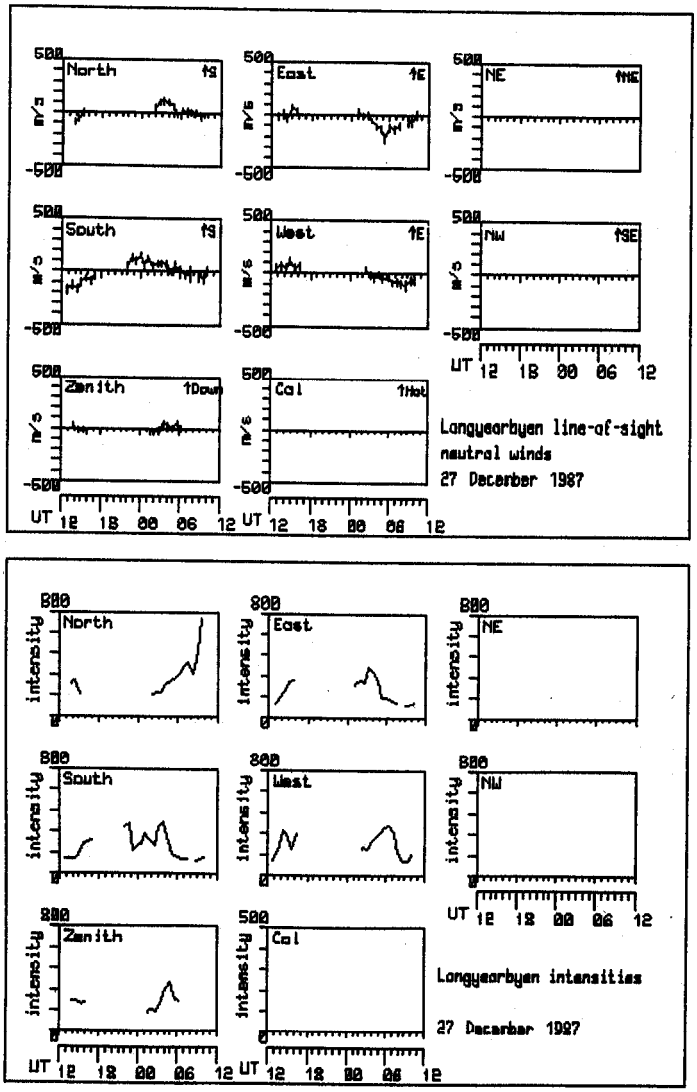

Figure 12. Thermospheric wind data from the Svalbard instrument on December 27, 1987, under relatively quiet geomagnetic activity conditions.

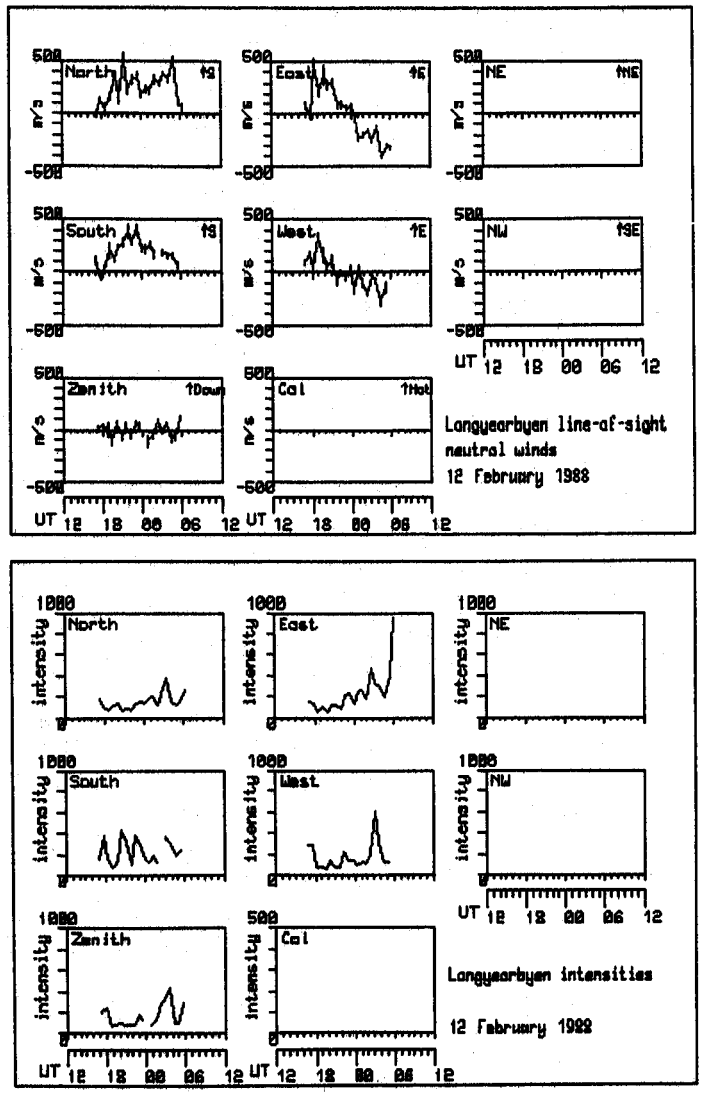

Figure 13. Thermospheric wind data from the Svalbard instrument on February 12, 1988, under very disturbed geomagnetic activity conditions.

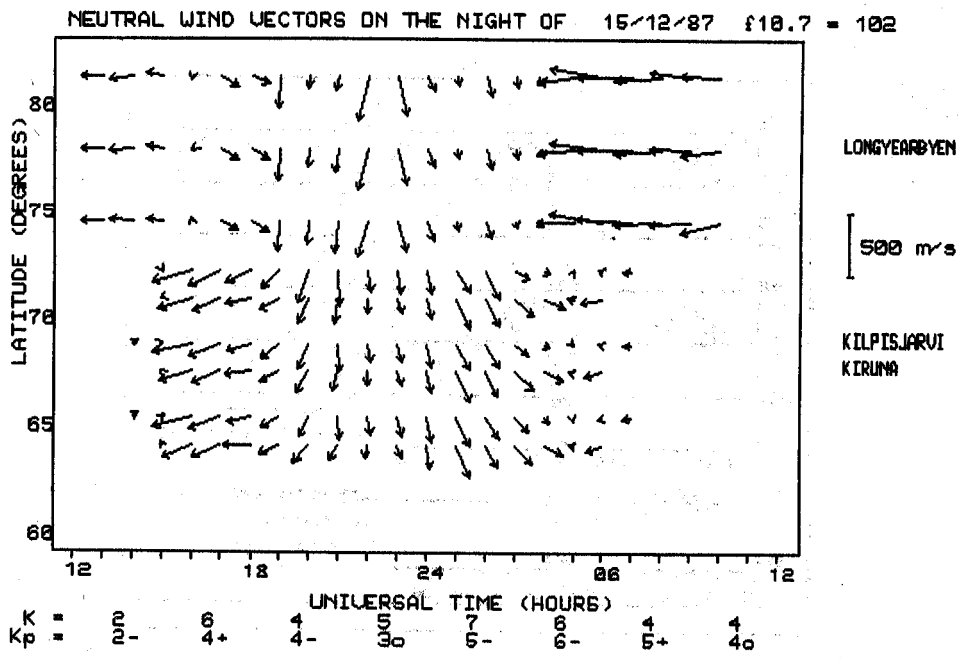

Figure 14. Thermospheric winds from three stations - Svalbard, Kilpisjarvi and Kiruna obtained on December 15 / 16, 1987, a moderately disturbed day.

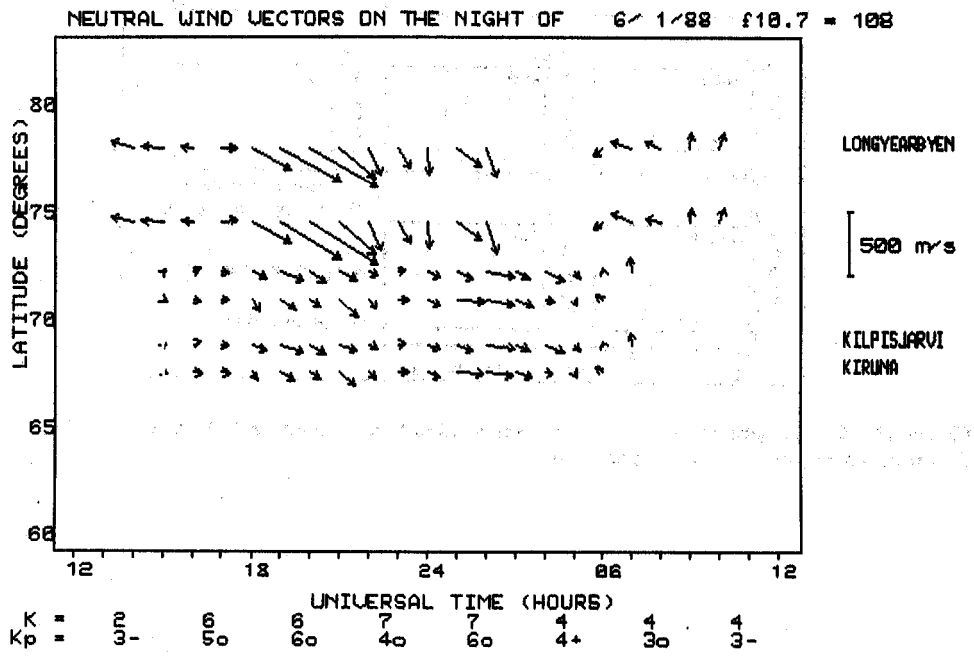

Figure 15. Thermospheric winds from three stations - Svalbard, Kilpisjarvi and Kiruna obtained on January 6 / 7 1988, a moderately disturbed day.

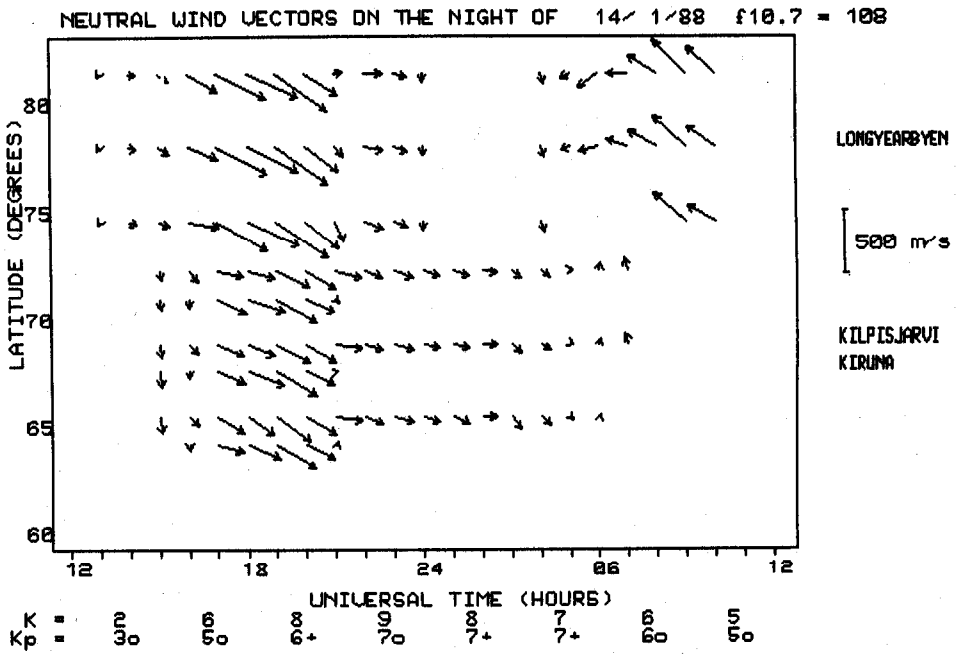

Figure 16. Thermospheric winds from three stations - Svalbard, Kilpisjarvi and Kiruna obtained on January 14 / 15, 1988. This was a very disturbed period, at a time when the auroral oval had expanded equatorward of Kiruna, even before the start of the observing period in the early afternoon.

unusual by virtue of the relative lack of coherence between the polar cap (Svalbard) and the two, relatively close (1000 km), auroral oval stations.

The data shown in Figure 16 was obtained during a very disturbed period, when the auroral oval had expanded equatorward of Kiruna before about 16 UT, in the early afternoon. The winds at all three stations are indicating very strong anti-sunward flow within a greatly-expanded polar cap. The response after 23 UT, at the height of the disturbance, and the recovery from this very disturbed period after about 05 UT were not observed so clearly due to a period of obscured sky at Svalbard. These data were also obtained during an unusual disturbance, and indicate the thermospheric response to a very high level of energy and momentum forcing within the greatly expanded auroral oval and polar cap.

Saskatoon: (52°N, 107°W, L=4.3)

The Imaging FPI at Saskatoon was built for Prof. Don McEwen (Institute for Space and Atmospheric Studies), and has been routinely operated there by Dr. N.D. Lloyd. The Fabry-Perot interferometer at Saskatoon has measured 557.7 nm Doppler shifts since August 1986 and Doppler wind flow data on some thirty six clear nights, from October 1986 to June 1987, have been published (Lloyd et al., 1989). These data corresponded to the period near solar minimum, and presented an opportunity to study the quiet thermosphere.

Utah State University: (42°N, 110°W)

During mid 1988, an Imaging FPI belonging to UCL was installed at Center for Atmospheric and Space Science (CASS) at Utah State University. Dr. Robert Sica and Dr. Vince Wickwar are the local scientists who have been responsible for all of the accommodation and installation arrangements. Initially, the instrument was operated from the roof of CASS, close to down-town Logan, studying OI 630 nm, while awaiting a GaAs IPD from ITT. That device was installed in August / September 1989. Since then, the instrument has been moved to a dark-sky site at Hardware Ranch / Bear Lake, and the instrument is now routinely observing mesospheric winds using the OH Mienel emissions at 843/845 nm. Initial data from this system are presented in Figures 17 and 18.

In Figure 17, the OI 630 nm winds are displayed for a very disturbed night, August 29, 1989. In the local midnight period, the equatorward wind reaches 500 ms^{-1}, with a 200 - 300 ms^{-1} westward component as well. Considering the geomagnetic location of the USU station, the wind response is due to ion drag and heating in a greatly expanded auroral oval, with a very large cross-polar cap potential. The auroral oval did not expand quite as far equatorward as the FPI station, but bright aurora were observed in the northern part of the sky for much of the period of FPI observations. These data were obtained with the FPI immediately (2 hrs) after installation of the GaAs IPD.

In Figure 18, some data obtained on the OH 843/845 nm emissions with the new GaAs IPD are presented (Rees et al., 1989). The wind scale for these data is 50 ms^{-1}, rather than the 500 ms^{-1} used to present the thermospheric wind results. Although only some 5 nights of data on OH winds have yet been analysed, the mesospheric wind flows (around 85 km altitude) present a pattern of considerable day to day regularity, indicating tidal amplitudes of the order of 30 - 50 ms^{-1}. These can be readily seen in Figure 18. There are some very interesting day to day variations, and times when on particular nights, short term fluctuations of winds and intensity occur. It was not possible to run the stabilised single-mode He-Ne laser during this period of observations, however, when that is commissioned in the very near future, the regular calibration of the instrument function will permit mesospheric temperatures to be derived, in addition to sustaining the study of the upper mesospheric winds, of which these are the first results.

The Doppler Imaging System: (IRF, 67° N, 22°E)

The DIS is located at Kiruna, and has been described previously. In its initial configuration, the data handling and data analysis operations were extremely burdensome. Recently, with a dedicated PC, and large disk, plus some improved methods of calibration and data analysis, it has been possible to run the

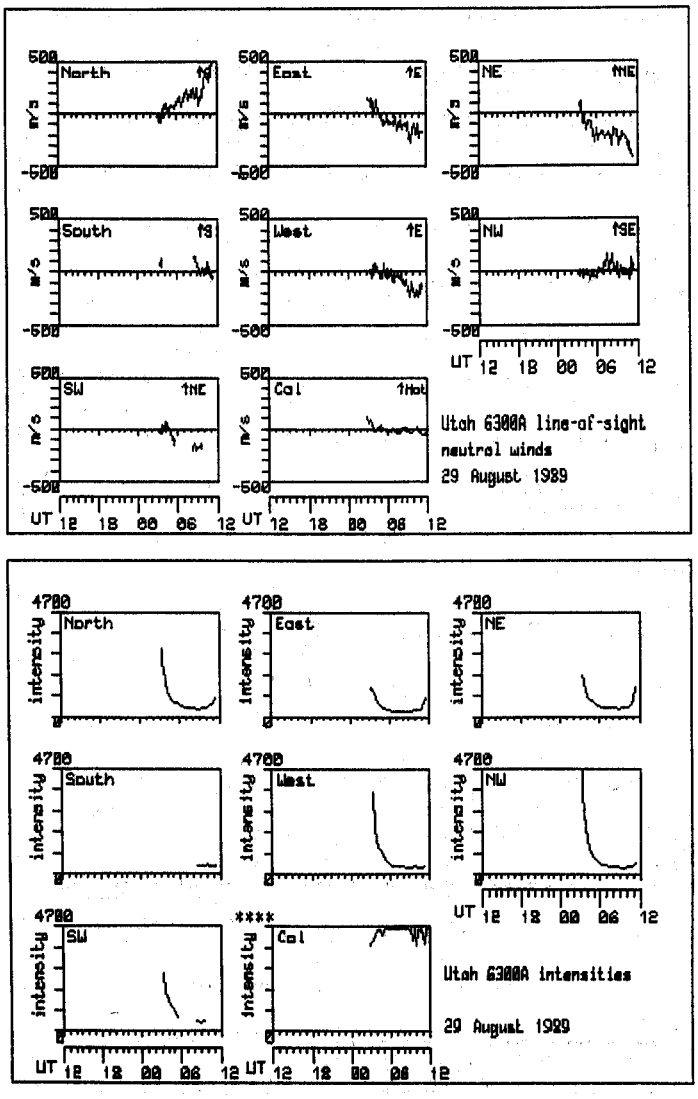

Figure 17. Initial Thermospheric wind data from the Imaging FPI at CASS, Utah, observing OI at 630 nm are presented. The data correspond to a major geomagnetic disturbance on August 29/30 1989.

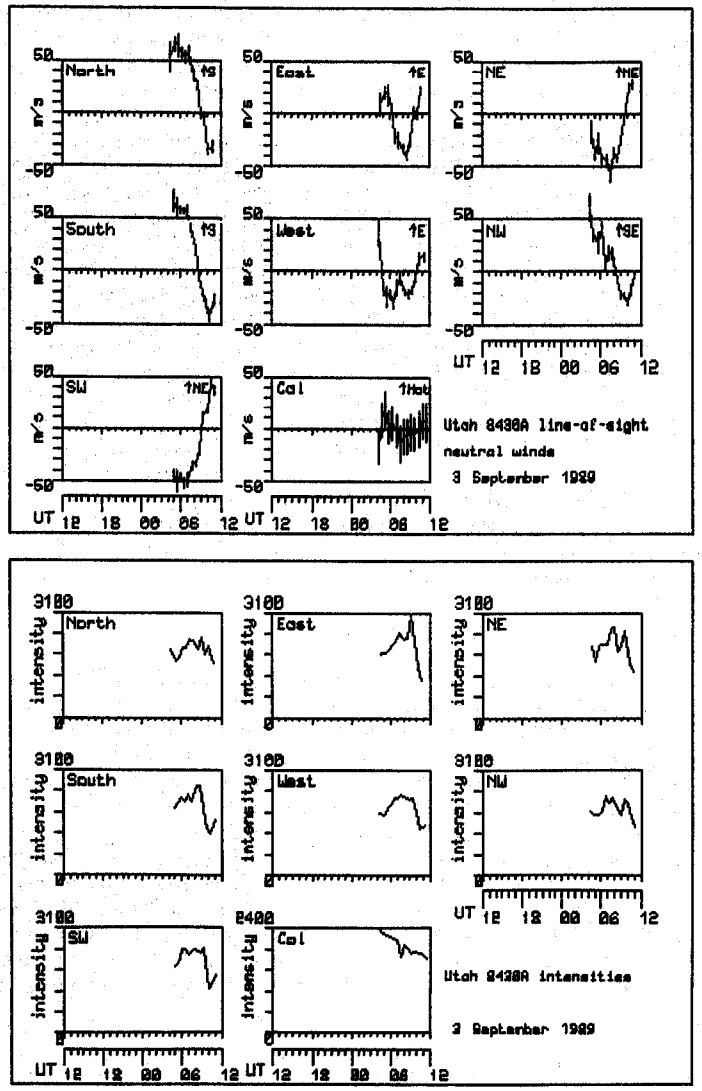

Figure 18. Initial mesospheric wind data from the Imaging FPI at Bear Lake, Utah observing OH at 843/845 nm are presented (September 3/4, 1989). There is a relatively regular 'tidal' behaviour of these winds from night to night, although wave-like features are also observed.

instrument on a routine basis. It has still, however, proven impractical to fully analyse the entire data set available. The full data sets are normally given an initial analysis, and are then archived. The data from the standard FPI is then usually used to determine a sub-set of those nights during which the more interesting thermospheric / auroral events may have occurred. With an initial selection, the full data analysis, which is a heavy user of time, computing effort and graphical hard-copy, can then be applied with rather greater efficiency. This instrument is due for a significant upgrade in the 1989 / 1990 winter: all-sky optics, detector and spectral calibration system.

Some of the data from the DIS were displayed earlier. In Figures 19 and 20, data from two disturbed nights are shown (Batten et al., 1990). Figure 19 shows data from the period 15:30 to 16:30 UT on the afternoon of December 21, 1987. There is a very large geomagnetic disturbance in progress, causing the bright OI 630 nm emissions, and the fast (500 ms^{-1}) westward winds. There are two distinct maxima in the westward wind speeds, the first near 16 UT, and the second around 16:40 UT. In Figure 20, a slightly different presentation is used to display a summary of the winds along the 20 degree east meridian, for the entire night of Dec 16 / 17 (UT) 1987. Many of the classical features of the thermospheric wind response on a night of moderate auroral and geomagnetic activity can be observed: westward winds in the dusk period, strong auroral disturbances around 16-18 UT, a rotation of the wind vector to southward and southeastward between 18 and 01 UT, and a general reduction of wind speed toward the dawn period. Just before dawn, as the auroral oval moves well poleward of Kiruna, a combination of local time effect and the general reduction of geomagnetic activity (the K index is plotted above the corresponding wind data), the winds turn anti-sunward, i.e. toward the northwest.

We are also in the process of developing a second DIS unit, which is intended to be mobile: to be used at various locations on a campaign basis. This system will probably use a Gallium Arsenide IPD, as available from ITT. As the DIS is applied to spectral targets other than OI 630 nm, we can expect that some very interesting new results will be obtained.

Acknowledgements:

The authors wish to recognise the contributions of Keith Smith and Jim Percival, in particular, to the development of the Fabry-Perot Interferometers and the Doppler Imaging System, and to Ake Steen, in particular, for general on-site support, and for maintaining the regular operation of the various instruments at IRF, Kiruna. The late Mr. Harenkowski provided continuous support for the instrument at Kilpiskarvi, a role recently continued by his wife. Dr. Risto Pellinen of Met. Inst. Helsinki, Dr. Kjell Henricksen of Tromso University, Dr. Robert Sica and Dr. Vince Wickwar of CASS, Utah State University provided the great deal of support required to get the optical facility set up at the CASS and recently the Hardware Ranch / Bear Lake Site in Utah. The instruments were all fabricated at UCL. With the exception of the Saskatchewan and Halley Bay instruments, their fabrication and the UCL aspects of their operation and the data analysis etc have been partly funded through grants from the UK Science and Engineering Research Council. The contributions of IRF, Kiruna, Tromso University (Svalbard) and CASS (Utah State University) to the maintenance of the facilities and routine operation of the respective instruments is gratefully acknowledged.

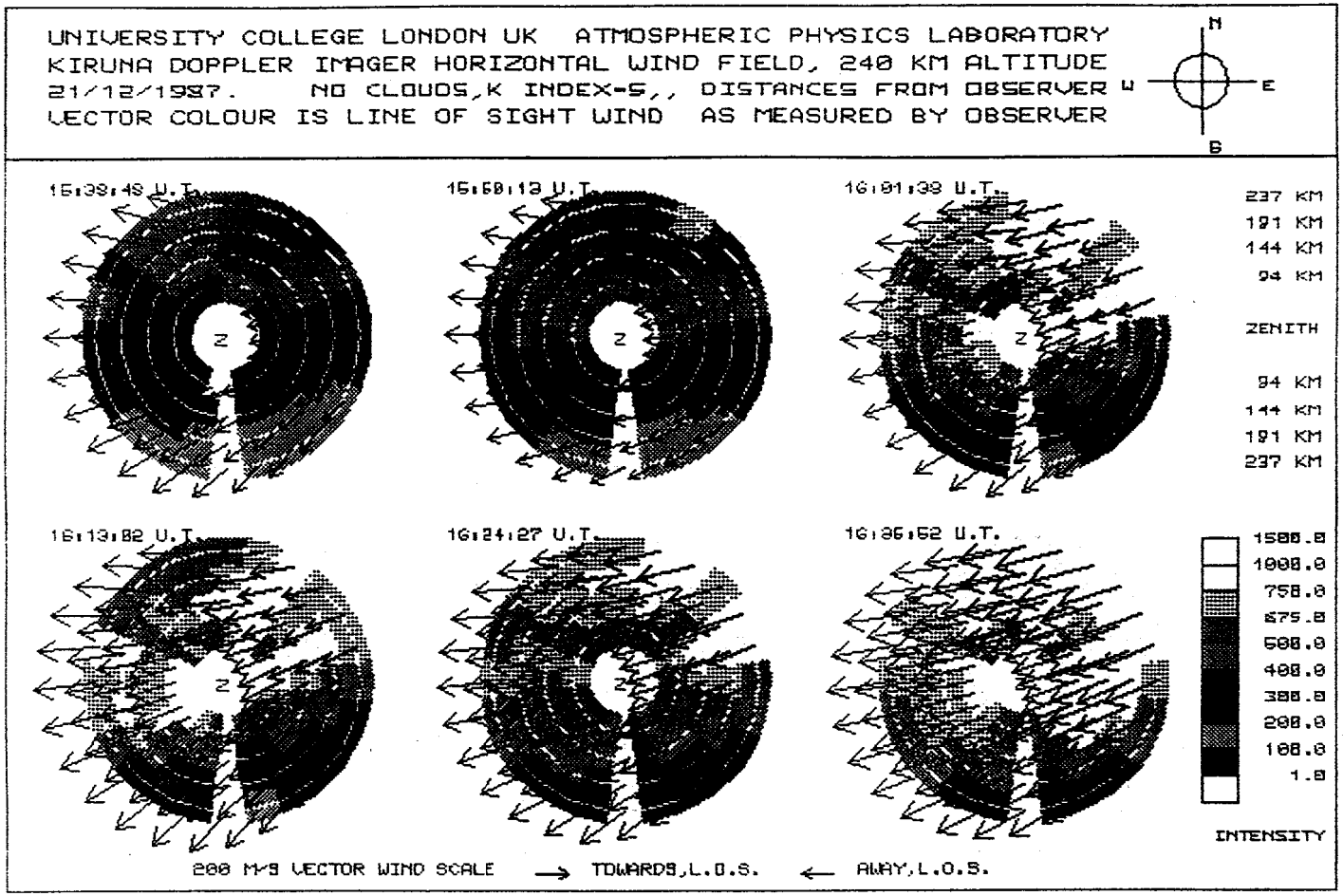

Figure 19. Data from the DIS at Kiruna during the disturbed night December 21, 1987.

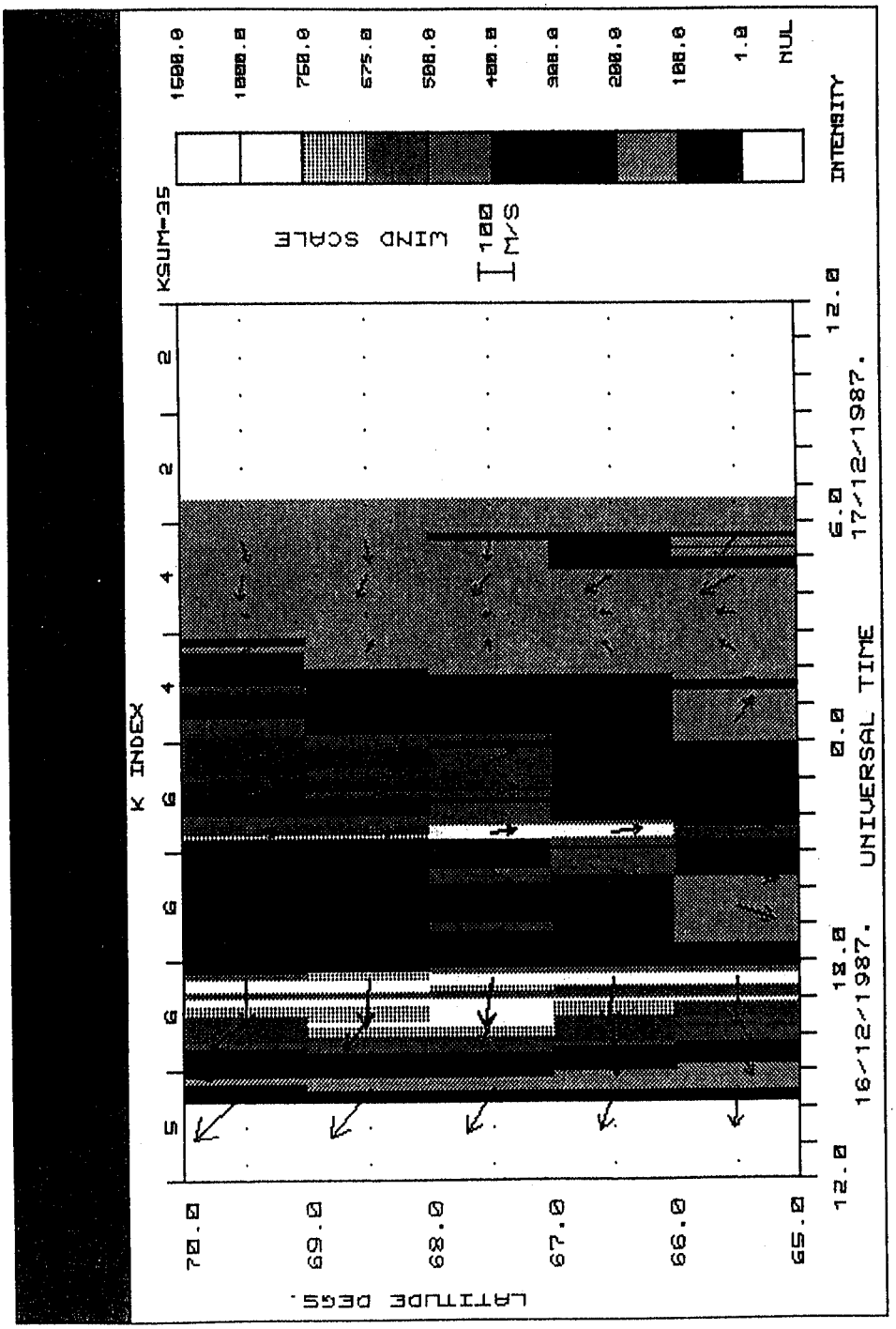

Figure 20. Data from the DIS at Kiruna during the disturbed night December 16, 1987.

References

Abreu V. J., G. A. Schmitt, P. B. Hays, J. W. Meriwether, C. A. Tepley and L. L. Cogger (1983). "Atmospheric scattering effects on ground-based measurements of thermospheric winds". Planet. Space Sci., 31, 303-310.

Armstrong E. B. (1968). "Variations in the width of the OIλ5577 line night airglow". Planet. Space Sci., 16, 211-229.

Aruliah A., D. Rees and T. J. Fuller-Rowell (1990). "The Combined Effect of Solar and Geomagnetic Activity on High Latitude Thermospheric Neutral Winds". Paper presented at the IAGA meeting in Exeter, July 1989, to be published in a special issue of Jn. Atmos. Terr. Phys.

Aruliah A. (1990), "The Synoptic Variety of the Thermosphere and Mesosphere Winds observed using a Fabry-Perot Interferometer". Ph. D. Thesis, University of London.

Batten S. M., D. Rees, D. Wade and A. Steen (1988). "Observations of thermospheric neutral winds by the UCL Doppler Imaging System at Kiruna in northern Scandinavia". J. Atmos. Terr. Phys. Vol 50, No 10/11, p861-888.

Batten S. M., and D. Rees (1990). "Thermospheric Winds in the Auroral Oval: Observations of small scale structures and rapid fluctuations by a Doppler Imaging System". J. Atm. Terr. Phys. (in press).

Burch S. F., S. F. Gull and J. Skilling (1983). "Image restoration by a powerful maximum entropy method". Computer Vision, Graphics, and Image Processing 23, p113-128.

Fuller Rowell T. J., D. Rees, S. Quegan, R. J. Moffett and G. J. Bailey (1987). "Interactions between Neutral Thermospheric Composition and the Polar Ionosphere using a Coupled Ionosphere-Thermosphere Model". J. Geophys. Res. 92, p7744-48.

Gull S. F. and G. J. Daniell (1978). "Image reconstruction from incomplete and noisy data". Nature, 272, p686-690.

Gull S. F. and J. Skilling (1984). "Maximum entropy method in image processing". IEE Proc, Vol 131, p646-659.

Hernandez G. (1986). Fabry-Perot interferometers. Cambridge University Press.

Kaskiewicz, P., (1978). "Interferometric Observations of Airglow Emissions from Space Vehicles", Phd. Thesis, University of London.

Killeen T. L., P. B. Hays, B. C. Kennedy and D. Rees (1982). "Stable and rugged etalon for the Dynamics Explorer Fabry-Perot Interferometer: II. Performance". Appl. Opt., 21, 3903-3912.

Killeen T. L., P. B. Hays, N. W. Spencer and L. E. Wharton (1982). "Neutral winds in the thermosphere as measured by Dynamics Explorer". Geophys. Res. Lett. 9, 957-960.

Killeen T. L. and P. B. Hays (1984). "Doppler line profile analysis for a multichannel Fabry-Perot interferometer", Appl. Opt., 23, 612-620.

Lloyd N. D. (1985). "Measurement of Neutral Thermospheric Winds using Ground-Based Fabry-Perot Interferometers", Ph. D. Thesis, University of London.

Lloyd N. D., D. J. McEwen, G. S. Sofko and D. Rees (1989). "Observations of 557.7 nm neutral winds from October 1986 to June 1987 using a ground-based Fabry-Perot interferometer at Saskatoon, Canada (52^{O}N, 107^{O}W)". J. Geophys. Res., in press.

McWhirter I., D. Rees and A. H. Greenaway (1982). "Miniature imaging photon detectors. III. An assessment of the performance of the resistive anode IPD". J. Phys. E: Sci. Instrum., 15, p145-150.

Meriwether J. W., Jr., P. Shih, T. L. Killeen, V. B. Wickwar and R. G. Roble (1984). "Nighttime thermospheric winds over Sondre Stromfjord, Greenland". Geophys. Res. Lett., 9, 931-934.

Meriwether J. W., Jr., J. W. Moody, M. A. Biondi and R. G. Roble (1986). "Optical interferometric measurements of winds at Arequipa, Peru". J. Geophys. Res., 91, 5557-5566.

Meriwether J. W., Jr. (1989). "Ground-based Fabry-Perot Interferometers": This Issue.

Rees D. (1979). "Remote Sensing of Middle Atmosphere Winds from Balloon Platforms". (COSPAR) Scientific Ballooning. Ed. W. Reidler, Pergammon Press, 207-210.

Rees D., I. McWhirter, P. A. Rounce, F. E. Barlow and S. J. Kellock (1980). "Miniature imaging photon detectors". J. Phys. E: Sci. Instrum., 13, 763-770.

Rees D., I. McWhirter, P. A. Rounce and F. E. Barlow (1981). "Miniature imaging photon detectors II. Devices with transparent photocathodes". J. Phys. E: Sci. Instrum., 14, 229-233.

Rees D., T. J. Fuller-Rowell, A. Lyons, T. L. Killeen and P. B. Hays (1982). "Stable and rugged etalon for the Dynamics Explorer Fabry-Perot Interferometer: I. Design and Construction". Applied Optics 21, 3896-3902.

Rees D. and A. H. Greenaway (1983). "The Doppler Imaging System: An optical device for measuring vector winds. I. General Principles". Applied Optics 22, 1078-1083.

Rees D., T. J. Fuller-Rowell, R. Gordon, T. L. Killeen, P. B. Hays, L. E. Wharton and N. W. Spencer (1983). "A Comparison of Wind Observations of the Upper Thermosphere from the Dynamics Explorer Satellite with the Predictions of a Global Time-Dependent Model". Planet. Space Sci. 31, 1299-1314.

Rees D., A. H. Greenaway, R. Gordon, I. McWhirter, P. J. Charleton and A. Steen (1984). "The Doppler Imaging System : Initial observations of the auroral thermosphere". Planet. Space Sci. 32, p273-285.

Rees D., R. W. Smith, P. J. Charleton, F. G. McCormac, N. D. Lloyd and A. Steen (1984a). "The generation of vertical thermospheric winds and gravity waves at auroral latitudes, I, Observations of thermospheric winds". Planet. Space Sci. 32, 667-684.

Rees D., M. F. Smith and R. Gordon (1984b). "The Generation of Vertical Thermospheric Winds and Gravity Waves at Auroral Latitudes, II, Theory and Numerical Modelling of Vertical Winds". Planet. Space Sci. 32, 685-705.

Rees D., N. D. Lloyd, P. J. Charleton, M. Carlson, J. Murdin and I. Haggstrom, (1984c). "Comparison of Plasma Flow and Thermospheric Circulation over Northern Scandinavia using EISCAT and a Fabry-Perot Interferometer". J. Atmos. Terr. Phys. 46, 545-564.

Rees D., R. Gordon, T. J. Fuller-Rowell, M. F. Smith, G. R. Carignan, T. L. Killeen, P. B. Hays and N. W. Spencer (1985). "The Composition, Structure, Temperature and Dynamics of the Upper Atmosphere in the Polar Regions during October to December 1981". Planet. Space Sci. 33, 617-666.

Rees D., T. J. Fuller-Rowell, R. Gordon, M. F. Smith, J. P. Heppner, N. C. Maynard, N. W. Spencer, L. Wharton, P. B. Hays and T. L. Killeen (1986). "A Theoretical and Empirical Study of the Response of the High Latitude Thermosphere to the Sense of the 'Y' Component of the Interplanetary Magnetic Field". Planet. Space Sci. 34, 1-40.

Rees D., N. D. Lloyd, T. J. Fuller-Rowell and A. Steen (1987). "Variations of thermospheric winds in northern Scandinavia between 1980 and 1986: a study of geomagnetic activity effects during the last solar cycle". Surv. Geophys. 9, 197-214.

Rees D., V. B. Wickwar and R. J. Sica (1989). "First OH (λ = 843 nm) Observations from the Bear Lake Site of the Hardware Ranch Observatory using a GaAs Imaging Photon Detector, Abstract for fall AGU meeting, 1989". EOS, Trans. Am. Geophys. Union.

Sibisi S. (1983). "Two-dimensional reconstructions from one-dimensional data by maximum entropy". Nature, Vol. 301, p134-137.

Skilling J. and R. K. Bryan (1984). "Maximum entropy image reconstruction: general algorithm". Mon. Not. R. Astr. Soc. 211, p111-124.

Smith R. W. and P. J. Sweeney (1980). "Winds in the thermosphere of the northern polar cap". Nature, 284, p437-438.

Steele D. P. and D. J. McEwen (1988). "Electron auroral excitation efficiencies and intensity ratios". Submitted to J. Geophys. Res.

Stewart R. D., R.W. Smith, D. Rees, A. S. Rodger and J. R. Dudeney (1985). "First Measurements of Thermospheric winds in Antarctica by an Optical Ground-based Method". Nature, 317, 45-47.

Stewart R. D., A. S. Rodger and J. R. Dudeney (1988). "Thermospheric wind response to driving forces in the vicinity of the Harang discontinuity". Planet. Space Sci., 36, 225-229.